High-throughput profiling of sequence recognition by tyrosine kinases and SH2 domains using bacterial peptide display

Allyson Li[1], Rashmi Voleti[1], Minhee Lee[1], Dejan Gagoski[1,2], Neel H. Shah[1,*]

[1] Department of Chemistry, Columbia University, New York, NY 10027

[2] Department of Biological Sciences, Columbia University, New York, NY 10027

* corresponding author: neel.shah@columbia.edu

ORCiDs

Allyson Li: 0000-0003-2359-7703

Rashmi Voleti: 0000-0002-3705-7460

Minhee Lee: 0000-0002-7141-7351

Dejan Gagoski: 0000-0001-6194-8514

Neel H. Shah: 0000-0002-1186-0626

Abstract

Tyrosine kinases and SH2 (phosphotyrosine recognition) domains have binding specificities that depend on the amino acid sequence surrounding the target (phospho)tyrosine residue. Although the preferred recognition motifs of many kinases and SH2 domains are known, we lack a quantitative description of sequence specificity that could guide predictions about signaling pathways or be used to design sequences for biomedical applications. Here, we present a platform that combines genetically-encoded peptide libraries and deep sequencing to profile sequence recognition by tyrosine kinases and SH2 domains. We screened several tyrosine kinases against a million-peptide random library and used the resulting profiles to design high-activity sequences. We also screened several kinases against a library containing thousands of human proteome-derived peptides and their naturally-occurring variants. These screens recapitulated independently measured phosphorylation rates and revealed hundreds of phosphosite-proximal mutations that impact phosphosite recognition by tyrosine kinases. We extended this platform to the analysis of SH2 domains and showed that screens could predict relative binding affinities. Finally, we expanded our method to assess the impact of non-canonical and post-translationally modified amino acids on sequence recognition. This specificity profiling platform will shed new light on phosphotyrosine signaling and could readily be adapted to other protein modification/recognition domains.

Introduction

Cells respond to external stimuli by activating a finely-tuned cascade of enzymatic reactions and protein-protein interactions. This signal transduction is governed, in large part, by post-translational modifications that alter protein activity, stability, and localization, as well as the formation of higher-order macromolecular complexes. Despite its low abundance relative to serine and threonine phosphorylation, tyrosine phosphorylation is an essential post-translational modification in metazoans (Lim and Pawson, 2010). Tyrosine kinases, the enzymes that phosphorylate tyrosine residues on proteins, and Src homology 2 (SH2) domains, protein modules that bind tyrosine-phosphorylated sequences, must have the ability to discriminate among a myriad of potential phosphorylation sites (phosphosites) in the proteome, in order to ensure proper signal transduction. The preferential engagement of specific phosphosites by tyrosine kinases and SH2 domains is dependent on the amino acid sequence surrounding the tyrosine or phosphotyrosine residue (Songyang et al., 1995, 1993).

Isolated tyrosine kinase domains most efficiently engage phosphosites that conform to specific sequence motifs, which are defined by a small number of key residues that contribute significantly to recognition (Songyang et al., 1995). These motifs suggest a mechanism by which a specific set of phosphosites in a proteome is selectively engaged by an individual kinase, based on the presence of favorable sequence features around that site. Negative selection of specific sequence features can also play a role in kinase specificity (Alexander et al., 2011). For example, the T cell tyrosine kinase ZAP-70 cannot readily phosphorylate co-localized proteins that contain even a modest positive charge (Shah et al., 2016).

Phosphosite sequence recognition by kinase domains is just one mechanism of substrate selection for tyrosine kinases, and other interactions are necessary to achieve efficient substrate targeting *in vivo*. Binding domains, such as SH2 domains, can strongly influence specificity by localizing kinases to the vicinity of phosphorylation targets (Pawson and Nash, 2000). Secondary interactions between SH2 and kinase domains can also refine the substrate preferences of a tyrosine kinase by stabilizing its active state (Filippakopoulos et al., 2008). Thus, for signaling systems that involve a tyrosine kinase domain and a tethered SH2 domain, the sequence specificities of both domains contribute to the intricate control of phosphotyrosine signaling responses.

Many methods have been developed to characterize sequence recognition by tyrosine kinases and SH2 domains. The most prominent approach employs purified kinases/SH2 domains and oriented peptide libraries, which are synthetic, degenerate peptide libraries with a central tyrosine or phosphotyrosine residue (Songyang et al., 1995, 1994a, 1994b, 1993). Several variations on this technique have been reported to improve the throughput and quantification of sequence preferences (Deng et al., 2014; Huang et al., 2008; Hutti et al., 2004; Mok et al., 2010). Notably, this method is also applicable to serine/threonine kinases, and large swaths of the yeast and human kinomes have been characterized using oriented peptide libraries, providing significant insights into kinase-substrate recognition and phospho-signaling (Deng et al., 2014; Johnson et al., 2022; Mok et al., 2010; Songyang et al., 1995). Oriented peptide library screens have primarily been useful for determining the preference for each amino acid at a given position, independent of sequence context, but evidence suggests that some amino acid preferences may depend on the surrounding sequence (Cantor et al., 2018).

Several groups have developed strategies to compare the phosphorylation of specific sequences, rather than obtain position-averaged amino acid preferences from pooled degenerate libraries. Strategies include “one-bead-one-peptide” combinatorial libraries (Imhof et al., 2006; Lam et al., 1998; Ren et al., 2011; Sweeney et al., 2005; Trinh et al., 2013; Wavreille et al., 2007) and protein/peptide microarrays (Amanchy et al., 2008; Jones et al., 2006; Koytiger et al., 2013; Mok et al., 2009; Schutkowski et al., 2004; Uttamchandani et al., 2003). One-bead-one-peptide methods often require manual isolation and individual sequencing of positive (phosphorylated or SH2-bound) beads, making the method technically challenging. Microarrays offer the capacity to analyze thousands of discrete sequences and require small quantities of proteins, but their use can be limited by the high cost of reagents. As an alternative, several groups have conducted mass spectrometry proteomics on kinase-treated cell extracts or cells over-expressing a kinase of interest (Barber et al., 2018b, 2018a; Chou et al., 2012; Corwin et al., 2017;

Finneran et al., 2020; Lubner et al., 2018; Sugiyama et al., 2019). This strategy has enabled the identification of potential substrates and can also be used to infer position-specific amino acid preferences. This approach also has the added benefit that the kinase of interest is operating on intact proteins, rather than isolated peptides, but interpretation of the results can be convoluted by the presence of endogenous kinases.

Molecular display techniques, such as mRNA, phage, yeast, and bacterial display, have also been used for specificity profiling. Early investigations employed phage or mRNA display to profile tyrosine kinase and SH2 specificity. These methods were relatively low-throughput, as they relied on Sanger sequencing of individual clones (Cujec et al., 2002; Dente et al., 1997; Gram et al., 1997). The advent of deep sequencing technologies has transformed this style of specificity profiling, by enabling rapid, quantitative analysis of library composition without requiring the sequencing of individual clones. This was demonstrated recently in a series of studies that employed bacterial peptide display, fluorescence-activated cell sorting (FACS), and deep sequencing to profile tyrosine kinase and SH2 domain specificity (Cantor et al., 2018; Lo et al., 2019; Shah et al., 2018, 2016). A key facet of those investigations was the facile generation of peptide libraries tailored to specific mechanistic questions: these included scanning mutagenesis libraries derived from individual substrates (Shah et al., 2016), as well as diverse peptide libraries encoding known phosphosites in the human proteome (Shah et al., 2018).

In this report, we describe a high-throughput platform to profile the recognition of large peptide libraries by any tyrosine kinase or SH2 domain. Our approach uses biotinylated bait proteins (pan-phosphotyrosine antibodies or SH2 domains) and avidin-functionalized magnetic beads to isolate tyrosine kinase-phosphorylated bacterial cells, and is coupled to deep sequencing for a quantitative readout (Figure 1A). The use of magnetic bead-based separation, rather than FACS, permits simultaneous, benchtop processing of multiple samples and enables the analysis of larger libraries for less time and cost. Libraries can be custom-made for specific readouts: mutational scanning for structure-activity relationships, libraries derived from natural proteomes to answer specific signaling questions, or degenerate libraries for the generation of predictive models.

To demonstrate the versatility of our approach, we designed two new bacterial peptide display libraries that provide distinct insights into tyrosine kinase and SH2 sequence recognition. The first library contains 10^6-10^7 random 11-residue sequences with a central tyrosine (referred to as the **X_5-Y-X_5 library**). Screens with the X_5-Y-X_5 library recapitulate previously reported specificity motifs and can be used to generate highly efficient peptide substrates. The second library contains defined sequences spanning 3000 human tyrosine phosphorylation sites, along with 5000 variant sequences bearing disease-associated mutations and natural polymorphisms (referred to as the **pTyr-Var library**). Kinase and SH2 screens with the pTyr-Var library reveal hundreds of phosphosite-proximal mutations that significantly impact phosphosite recognition by individual protein domains. These datasets will be a valuable resource in the growing efforts to understand the functional impact of protein variants across the human population that may contribute to disease (Stein et al., 2019). Finally, we show that our peptide display platform is compatible with Amber codon suppression, enabling analysis of how non-canonical or post-translationally modified amino acids impact sequence recognition. Overall, the method described in this report provides an accessible, high-throughput platform to study the specificity of phosphotyrosine signaling proteins.

Results and discussion

<u>A bacterial display and deep sequencing platform to screen tyrosine kinases against large peptide libraries</u>

We expanded upon a previously established screening platform that combines bacterial display of genetically-encoded peptide libraries and deep sequencing to quantitatively compare phosphorylation efficiencies across a substrate library (Shah et al., 2016). In the published approach, peptides are displayed on the surface of *E. coli* cells as fusions to an engineered bacterial surface-display protein, eCPX (Rice and Daugherty, 2008), then phosphorylated by a purified kinase (Henriques et al., 2013).

Following this, the cells are labeled with a pan-phosphotyrosine antibody, and cells with high phosphorylation levels are separated by FACS. The DNA encoding the peptides is then amplified and analyzed by Illumina deep sequencing to determine the frequency of each peptide in the library before and after selection (Shah et al., 2018, 2016). In order to determine the phosphorylation efficiency of each peptide by a particular kinase, an enrichment score is determined by calculating the frequency of that peptide in the kinase-selected sample normalized to the frequency in the input sample.

While peptide libraries of virtually any composition can theoretically be screened using this approach, previous implementations focused on libraries containing less than 5000 peptides, due to the low throughput of FACS (Shah et al., 2018). In those experiments, the objective was to over-sample the library at the cell sorting step by a factor of 100-1000, to ensure that enrichment or depletion of every member of the library could be accurately quantified by deep sequencing. When multiple screens were conducted in parallel, the throughput of FACS limited experiments to small libraries (less than 5000 sequences). To improve the scalability and cost-effectiveness of this approach, we switched to a bead-based sorting method, using avidin-coated magnetic beads to enrich highly-phosphorylated cells, thus circumventing the need for FACS (Figure 1A). With this approach, the cells are instead labeled with

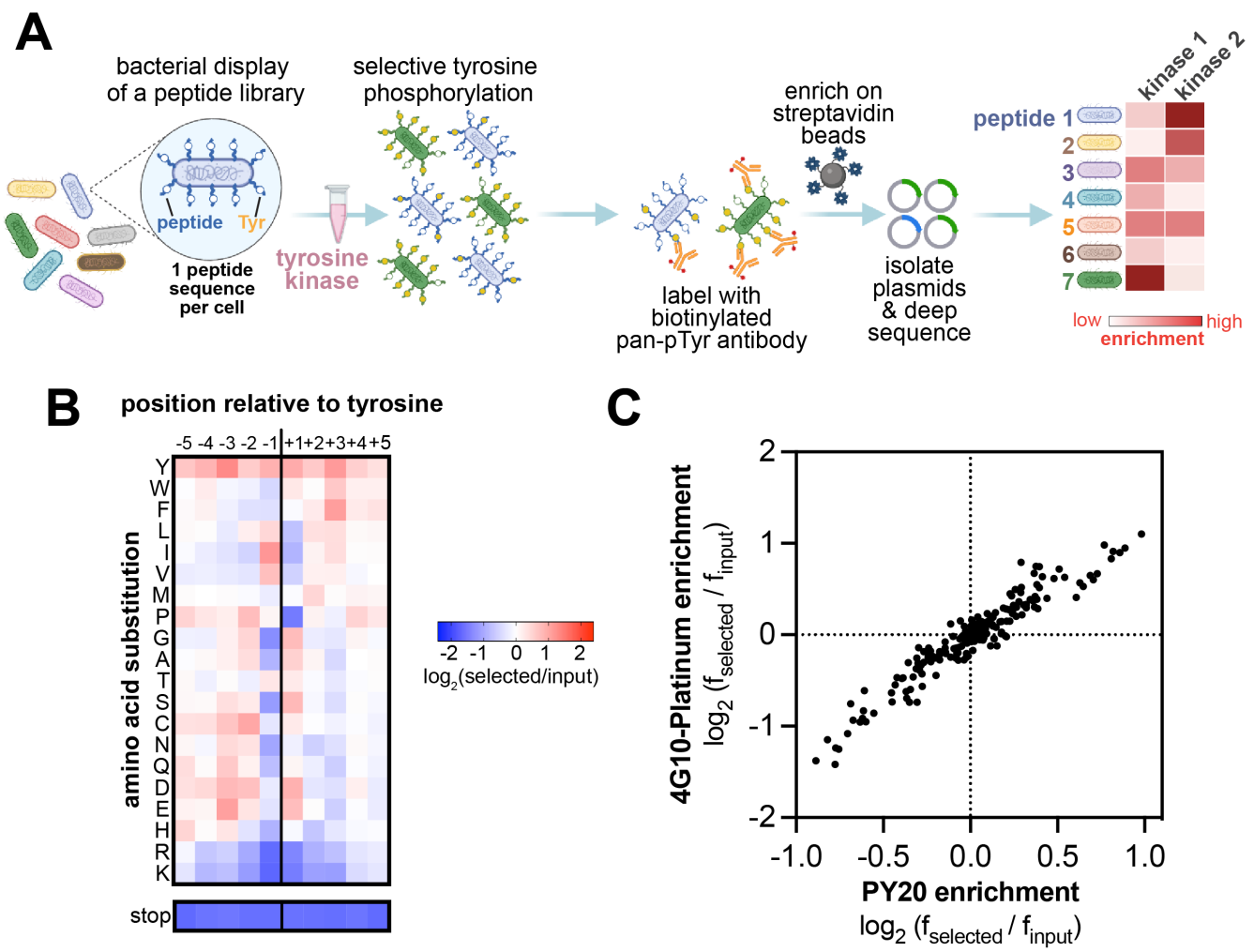

Figure 1. High-throughput profiling of tyrosine kinase substrate specificity using bacterial peptide display. (**A**) Schematic representation of the workflow for kinase specificity profiling. (**B**) Heatmap depicting the specificity of the c-Src kinase domain, measured using the X_5-Y-X_5 library. Enrichment scores were $\log_2$-transformed and are displayed on a color scale from blue (disfavored sequence features, negative value), to white (neutral sequence features, near zero value), to red (favored sequence features, positive value). Values in the heatmap are the average of three replicates. (**C**) Correlation between position-specific amino acid enrichments from screens with the 4G10 Platinum and PY20 biotinylated pan-phosphotyrosine antibodies.

biotinylated pan-phosphotyrosine antibodies and then sorted using magnetic beads. The use of magnetic beads permits simultaneous separation of multiple samples of virtually any size, enabling larger library analysis for less time and cost. Notably, these screens can be carried out in any laboratory, without the need for a fluorescence-activated cell sorter.

To test our upgraded screening platform, we generated a random library of 11-residue sequences with a central tyrosine (the X_5-Y-X_5 library, where X is any of the 20 canonical amino acids). The library was generated using a degenerate synthetic oligonucleotide with five NNS codons (N = A,T,G,C and S = G,C) before and after the central codon that encodes for tyrosine (TAT). The NNS triplet has the benefit of encoding all 20 amino acids, but it can still contain an Amber stop codon (TAG) roughly 3% of the time. Therefore, up to 30% of the peptide-coding sequences in the library are expected to have an Amber stop codon – a feature that we take advantage of later in this study. The degenerate oligonucleotide mixture was cloned into a plasmid in between the DNA encoding a signal sequence and the eCPX surface-display scaffold. In a previously reported version of this platform, the eCPX scaffold contained a C-terminal strep-tag to detect surface-display level (Shah et al., 2016). Due to the potential background binding of the strep-tag with the avidin-coated magnetic beads during cell enrichment, we cloned both a strep-tagged and a myc-tagged version of the library. Deep sequencing of both versions of the X_5-Y-X_5 library confirmed that they have 1-10 million unique peptide sequences, 20% of which contain one or more stop codons. Furthermore, all 20 canonical amino acids were well-represented at each of the 10 variable positions surrounding the fixed tyrosine residue (Figure 1-figure supplement 1).

Using the myc-tagged X_5-Y-X_5 library, we determined the position-specific amino acid preferences of the kinase domain of c-Src. Cells displaying the library were phosphorylated by c-Src to achieve roughly 20-30% phosphorylation, as determined by flow cytometry (Figure 1-figure supplement 2). The phosphorylated cells were enriched with magnetic beads, and peptide-coding DNA sequences were counted by deep sequencing. We visualized the sequence preferences of c-Src by generating a heatmap based on the position-specific enrichment scores of each amino acid residue surrounding the central tyrosine (Figure 1B). Sequences containing a stop codon were not considered in these calculations, but the depletion of stop codons at each position was separately confirmed and is reported below the heatmap on the same color scale. The preferences determined from this screen matched the sequence specificity of c-Src defined by prior reports using oriented peptide libraries (Deng et al., 2014; Songyang et al., 1995). We observed a strong preference for bulky aliphatic residues (Ile/Leu/Val) at the -1 position relative to the central tyrosine and a phenylalanine at the +3 position (Figure 1B). Our results showed modest differences from the specificity observed by oriented peptide libraries, including a strong preference for a +1 Asp/Glu/Ser in addition to the previously reported +1 Gly. To test whether these differences were due to biases introduced by the specific pan-phosphotyrosine antibody used, we obtained a different commercially available biotinylated pan-phosphotyrosine antibody and repeated the screen. The position-specific amino acid enrichments obtained using both antibodies were nearly identical (Figure 1C). This suggests that there is no significant bias in the enrichment of peptides introduced by the pan-phosphotyrosine antibody.

Degenerate library screens capture specificity profiles for diverse tyrosine kinases.

We next used the degenerate X_5-Y-X_5 library to characterize the sequence preferences of four additional tyrosine kinase domains, derived from the non-receptor tyrosine kinases c-Abl and Fer, and the receptor tyrosine kinases EphB1 and EphB2. The kinases were selected because they represent a few distinct branches of the tyrosine kinome and can be easily produced through bacterial expression (Albanese et al., 2018). The X_5-Y-X_5 library was screened against the kinases in triplicate, and the data from replicates were averaged to generate specificity profiles for each kinase (Figure 2A and Figure 2-source data 1). The amino acid preferences for c-Abl are well-characterized and were recapitulated in this screen (Deng et al., 2014; Songyang et al., 1995; Till et al., 1999, 1994). Like c-Src, c-Abl preferred bulky aliphatic residues at the -1 position with respect to the central tyrosine. Unlike c-Src, c-Abl preferred an alanine at the +1 position and had a notably strong preference for proline at the +3 position (Figures 1B and 2A). Fer showed a specificity pattern distinct from both c-Src and c-Abl, which included a

preference for tryptophan residues at the +2, +3, and +4 positions. As expected, the closely-related EPHB1 and EPHB2 kinases had similar specificities, which included a unique preference for an asparagine at the -1 residue that was not present in the non-receptor tyrosine kinases tested (Figure 2A).

Degenerate library screens can be used to design highly-efficient peptide substrates.

Specificity profiling methods are often used to design consensus sequences that serve as optimal peptide substrates for biochemical assays and biosensor design (Deng et al., 2014; Lin et al., 2019; Songyang et al., 1995). We wanted to assess whether our method could also be used to generate high-efficiency substrates, and whether these would differ from sequences identified using oriented peptide libraries. To test this, we combined the most favorable amino acids in each position flanking the central

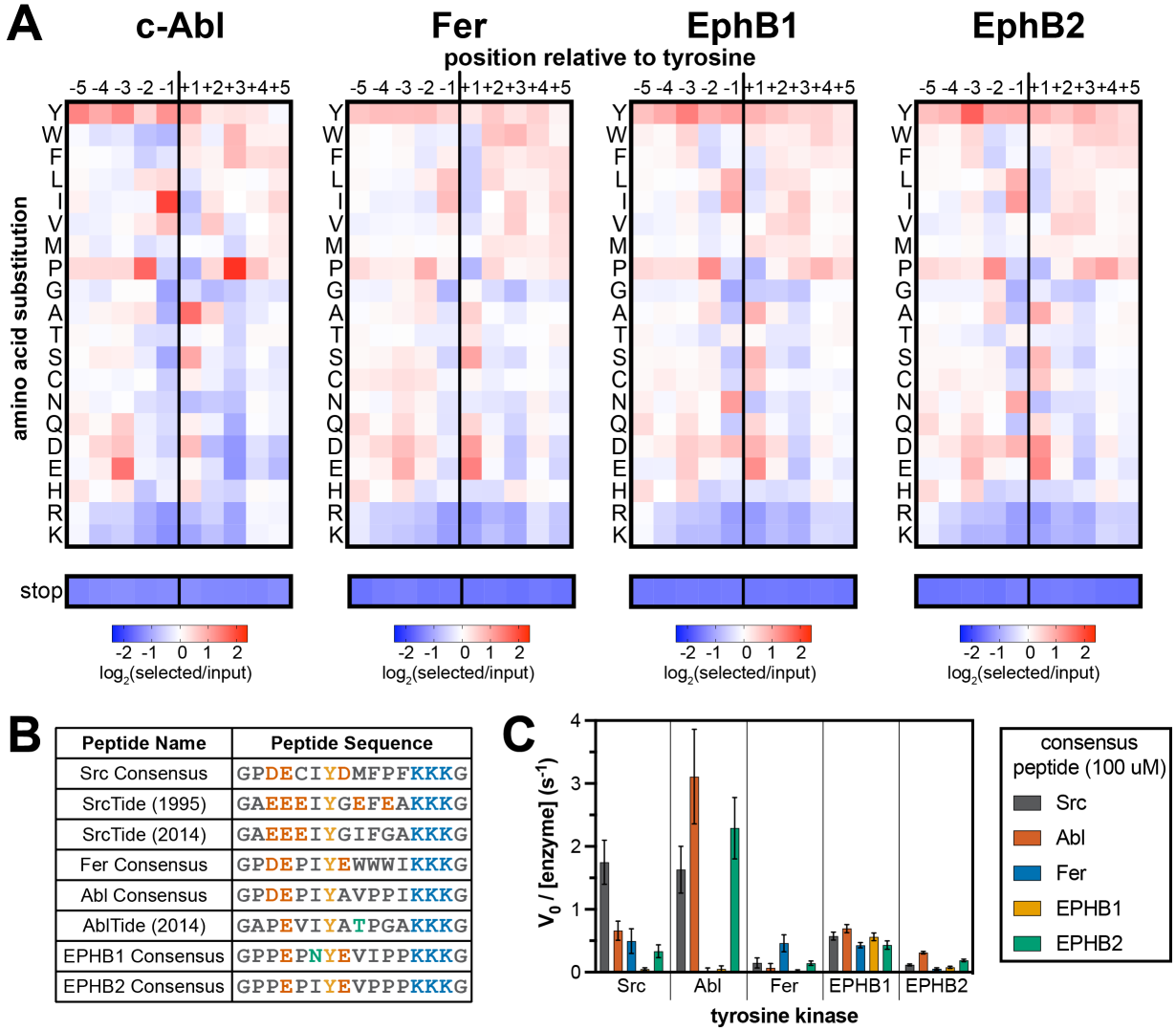

Peptide Name	Peptide Sequence
Src Consensus	GPDECIYDMFPFKKKG
SrcTide (1995)	GAEEEIYGEFEAKKKG
SrcTide (2014)	GAEEEIYGIFGAKKKG
Fer Consensus	GPDEPIYEWWWIKKKG
Abl Consensus	GPDEPIYAVPPIKKKG
AblTide (2014)	GAPEVIYATPGAKKKG
EPHB1 Consensus	GPPEPNYEVIPPKKKG
EPHB2 Consensus	GPPEPIYEVPPPKKKG

Figure 2. Specificity profiling of tyrosine kinases using the X_5-Y-X_5 library. (**A**) Heatmaps depicting the specificities of c-Abl, Fer, EPHB1, and EPHB2. Enrichment scores were log_2-transformed and are displayed on a color scale from blue (disfavored sequence features, negative value), to white (neutral sequence features, near zero value), to red (favored sequence features, positive value). Values in the heatmaps are the average of three replicates. (**B**) Sequences of consensus peptides identified through X_5-Y-X_5 screens, compared with previously reported SrcTide and AblTide sequences. (**C**) Phosphorylation kinetics of five consensus peptides against five kinases. All peptides were used at a concentration of 100 μM, and the kinases were used at a concentration of 10-50 nM. Error bars represent the standard deviation from at least three measurements.

tyrosine residue in our specificity profiles, excluding tyrosine, to generate unique consensus peptide substrates for c-Src, c-Abl, Fer, EPHB1, and EPHB2. Consensus sequences for c-Src and c-Abl have been identified previously using oriented peptide libraries (Deng et al., 2014; Songyang et al., 1995). These sequences, often referred to as SrcTide and AblTide, are different than our consensus sequences at a few residues surrounding the phospho-acceptor tyrosine (Figure 2B). The SrcTide and AblTide peptides are canonically embedded within a conserved peptide scaffold containing N-terminal Gly and C-terminal $(Lys)_3$-Gly flanks. For direct comparison, we embedded our consensus peptides in the same scaffold and conducted a series of kinetic studies.

First, we used an *in vitro* continuous fluorimetric assay to compare the steady-state kinetic parameters (k_{cat} and K_M) for our c-Src and c-Abl consensus peptides with the SrcTide and AblTide peptides generated using oriented peptide libraries. The Michaelis-Menten parameters for our Src Consensus peptide were on par with one of the previously reported SrcTide substrates (SrcTide 1995, (Songyang et al., 1995)), but the K_M value for a more recently reported SrcTide variant (SrcTide 2014, (Deng et al., 2014)) was substantially tighter (Figure 2-figure supplement 1) . Our Src Consensus peptide had a higher maximal catalytic rate (k_{cat}) but a lower apparent binding affinity (K_M) when compared to both SrcTides. We were surprised to see that our Src Consensus peptide had a +1 Asp residue, as opposed to the +1 Gly residue in both SrcTides. Substitution of the +1 Asp for a Gly in a related peptide marginally improved the K_M value but reduced k_{cat} (Figure 2-figure supplement 1). These results indicate that our c-Src specificity screens may be tuned to select for peptides with a high k_{cat}, and that there is a trade-off between k_{cat} and K_M for c-Src substrate recognition. For c-Abl, our consensus peptide had both a higher maximal rate (k_{cat}) and tighter apparent affinity (K_M) relative to the previously reported AblTide peptide (Figure 2-figure supplement 1). Collectively, these experiments suggest that different methods may be biased toward slightly different realms of sequence space, and that there are multiple solutions to achieving high-efficiency phosphorylation.

Next, we assayed all of the consensus peptides generated using our approach against their cognate kinases, as well as the other kinases in our screens. For the non-receptor tyrosine kinases (c-Src, c-Abl, and Fer), the corresponding consensus peptides were the best substrates tested. At a higher substrate concentration (100 μM), c-Abl also efficiently phosphorylated the Src and EPHB2 consensus peptides (Figure 2C), but selectivity for the Abl Consensus improved at a lower concentration (20 μM), consistent with selectivity being driven by K_M for this set of peptides (Figure 2-figure supplement 1,2). By contrast, c-Src was highly selective for the Src Consensus peptide at high concentrations (Figure 2C), but showed significant off-target activity toward the Fer Consensus at low concentrations (Figure 2-figure supplement 2). Michaelis-Menten analysis of the Fer Consensus with c-Src revealed that it has a remarkably tight K_M for c-Src, with a low k_{cat} as a trade-off (Figure 2-figure supplement 1). Finally, we observed that the receptor tyrosine kinase EPHB1 showed very little selectivity across the consensus peptides and did not prefer its own cognate consensus sequence (Figure 2C and Figure 2-figure supplement 2). EPHB2, on the other hand, efficiently phosphorylated its own consensus peptide, as well as the Abl Consensus. Both of these sequences contain a -1 Ile and +3 Pro (Figure 2B,C). These experiments demonstrate the applicability of our bacterial peptide display method to the design of high-activity substrates. Our results also suggest that not all consensus peptides will be selective for their given kinase, as there can be overlap in substrate specificities.

<u>Data from X_5-Y-X_5 library screens can be used to predict the relative phosphorylation rates of peptides.</u>

Given that data from the X_5-Y-X_5 library screens could yield high-efficiency substrates, we investigated whether the same data could be used to quantitatively predict the relative phosphorylation rates of biologically interesting sequences. If so, this would be a potentially powerful tool for the identification of native substrates and the dissection of phosphotyrosine signaling pathways. Indeed, oriented peptide libraries have been applied extensively to predict the native substrates of protein kinases (Johnson et al., 2022; Miller et al., 2008; Obenauer et al., 2003). We are particularly interested in using high-throughput specificity screens to predict how mutations proximal to phosphorylation sites affect tyrosine kinase selectivity. The PhosphoSitePlus database documents thousands of missense mutations

within 5 residues of tyrosine phosphorylation sites, many of which are associated with human diseases or are human polymorphisms, but the functional consequences of most of these mutations are unexplored (Hornbeck et al., 2019, 2015; Krassowski et al., 2018; Landrum et al., 2018).

We used the c-Src X_5-Y-X_5 screening data to predict the relative phosphorylation rates of six peptide pairs, corresponding to reference and variant sequences derived from human phosphorylation sites. Each peptide sequence was scored using an approach that is similar to that used for oriented peptide libraries in the Scansite database (Obenauer et al., 2003; Yaffe et al., 2001). For each peptide sequence, we summed the $\log_2$-transformed enrichment values for the appropriate amino acid at each position in the peptide (the numerical values that make up the heatmaps in Figures 1B and 2A). This sum was divided by the number of variable positions (10 positions for all peptides in this study), then normalized to be on a scale from 0 (the worst possible sequence) to 1 (the best possible sequence). We compared the predicted scores to *in vitro* phosphorylation rates measured using a highly-sensitive assay based on reverse-phase high-performance liquid chromatography (RP-HPLC) (Figure 3 and Figure 3-figure supplement 1). We found that our predictions, which were derived from log-transformed enrichment scores, correlated moderately well with the log-transformed rates of phosphorylation by c-Src (Figure 3A). The predictions could differentiate high, medium, and low activity substrates but could not accurately rank peptides within these clusters. Focusing specifically on the effects of the mutations in this set of peptides, we found that the X_5-Y-X_5 screening data could accurately predict the directionality of the effects of five out of six mutations (Figure 3B).

One drawback to the aforementioned scoring approach, like all models based on position-specific scoring matrices, is that it cannot capture context-dependent amino acid preferences. We recently explored a machine-learning approach, using screening data from a related degenerate library, to model c-Src kinase specificity (Rube et al., 2022). The model not only incorporated pairwise inter-residue dependencies, but also data from multiple time points. This approach could reasonably predict absolute rate constants, as well as the directionality and magnitude of several phosphosite-proximal mutational effects. As an alternative to building models based on random library screens, we reasoned that direct measurements of reference and variant peptides using our screening platform might also provide reliable assessment of mutational effects.

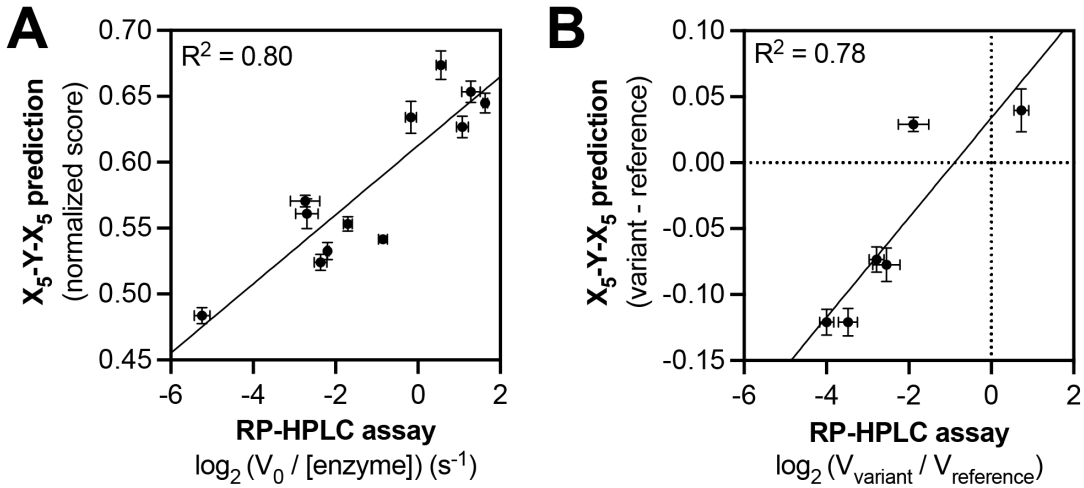

Figure 3. Predicting relative phosphorylation rates using data from X_5-Y-X_5 library screens. (**A**) Correlation between measured phosphorylation rates and X_5-Y-X_5 predictions for 12 peptides with c-Src. All peptides were used at a concentration of 100 μM, and c-Src was used at a concentration of 500 nM. Error bars represent the standard deviation from at least three rate measurements and three separate scores with individual replicates of the X_5-Y-X_5 screen. (**B**) Correlation between the magnitude of mutational effects for 6 peptide pairs with mutational effects predicted from X_5-Y-X_5 library screens. Error bars represent the standard deviation of at least three rate measurements and three separate scores with individual replicates of the X_5-Y-X_5 screen.

Natural variants of tyrosine phosphorylation sites impact kinase recognition.

To refine our assessment of phosphosite-proximal mutational effects, we designed a library, derived from the PhosphoSitePlus database, that is composed of 11-residue sequences spanning 3,159 human phosphosites and 4,760 disease-associated variants of these phosphosites bearing a single amino acid substitution (pTyr-Var library; Figure 4-figure supplement 1) (Hornbeck et al., 2019). While the majority of sequences in this library contained a single tyrosine residue, some sequences contained multiple tyrosines, for which we included additional variants where the non-central tyrosine residues were mutated to phenylalanine. Including these tyrosine mutants and additional control sequences, such as previously designed consensus substrates, the library totaled ~10,000 unique sequences. As with the X_5-Y-X_5 library, we generated two versions of this library, bearing a C-terminal strep-tag or myc-tag. We conducted specificity screens with the myc-tagged pTyr-Var library against 8 non-receptor tyrosine kinases (c-Src, Fyn, Hck, c-Abl, Fer, Fes, Jak2, and AncSZ, an engineered homolog of Syk and ZAP-70 (Hobbs et al., 2022)) and 5 receptor tyrosine kinases (EphB1, EphB2, FGFR1, FGFR3, and MERTK). A majority of these kinases could be expressed in bacteria and purified in good yield (Albanese et al., 2018; Hobbs et al., 2022). One of these kinases (Jak2) was purchased from a commercial vendor.

Using the catalytically active tyrosine kinase constructs, we identified an optimal concentration (typically between 0.1-1.5 μM) to ensure 20-30% of maximal phosphorylation in three minutes. For some kinases (FGFR1, FGFR3, and MERTK), pre-incubation with ATP was required in order to activate the kinase by auto-phosphorylation (Figure 4-figure supplement 2). We conducted the screens analogously to those with the X_5-Y-X_5 library, but rather than calculate position-specific residue preferences from the deep sequencing data, we directly calculated enrichment scores for each peptide in the pTyr-Var library (Figure 4A and Figure 4-source data 1). Three to five replicates of the pTyr-Var screen were conducted with each kinase, and the results were reproducible across replicates (Figure 4-figure supplement 3). To validate our pTyr-Var screens, we examined enrichment scores from the c-Src experiments for the same six peptide pairs for which predictions using X_5-Y-X_5 screening data were only moderately accurate. We found a strong correlation between the pTyr-Var enrichment scores and phosphorylation rates, particularly for high-activity sequences (Figure 4B). Furthermore, the effects of mutations in the screens were consistent with those observed using the *in vitro* RP-HPLC assay with purified peptides (Figure 4C).

374 peptides in the pTyr-Var library contain no tyrosine residues and thus serve as controls to determine background noise in our screens. For every kinase tested, the tyrosine-free sequences showed distinctly low enrichment scores, consistent with signal in these screens being driven by tyrosine phosphorylation of the surface-displayed peptides (Figure 4A). For each kinase, a subset of the library (between 7-10%) showed enrichment scores above this background level (Figure 4A). To confirm that the pTyr-Var screens were reporting on unique substrate specificities across these tyrosine kinases, we calculated Pearson's correlation coefficients for the average datasets of each kinase pair (Figure 4D). We found strong correlation in specificity between kinases of the same family (the Src-family kinases c-Src, Fyn, and Hck, and receptor pairs EPHB1/EPHB2 and FGFR1/FGFR3). We also observed that the specificity of Src-family kinases partly overlapped with the Ephrin receptors and MERTK. The specificity of AncSZ and Jak2 correlated with that of FGFRs. Unexpectedly, Fes and Fer differed quite a bit in their specificities despite being in the same subfamily, with Fer being more comparable to the Src-family kinases, ephrin receptors, and MERTK.

For pairs of peptides that corresponded to a disease-associated variant and a reference sequence, we calculated the $\log_2$-fold change in enrichment for the variant relative to the reference. The large number of replicates for each screen afforded a robust analysis of phosphosite-proximal mutational effects for each kinase. We filtered the results in five steps to identify significant mutations: (1) We omitted phosphosite pairs where there was no statistically significant difference in enrichment between the variant and reference (p-value cutoff of 0.05). (2) We then applied a second filtering step to remove phosphosite pairs where the fold-change in enrichment between the variant and reference sequence was less than two. (3) Next, we excluded pairs where both sequences were low-activity substrates (enrichment score less than 1.5). (4) We removed mutations that added or removed a tyrosine residue, as their interpretation is ambiguous in our assay. (5) Lastly, we excluded phosphosite pairs in which the average read count of either the variant or wild-type sequence was less than 50. This left us with unique set of 50-400 high-

confidence candidates for each tyrosine kinase (Figure 4E, Figure 4-figure supplement 4, and Figure 4-source data 1). Notably, kinases had distinct patterns of mutational sensitivity at each position around the central tyrosine, consistent with distinct sequence preferences (Figure 4-figure supplement 5).

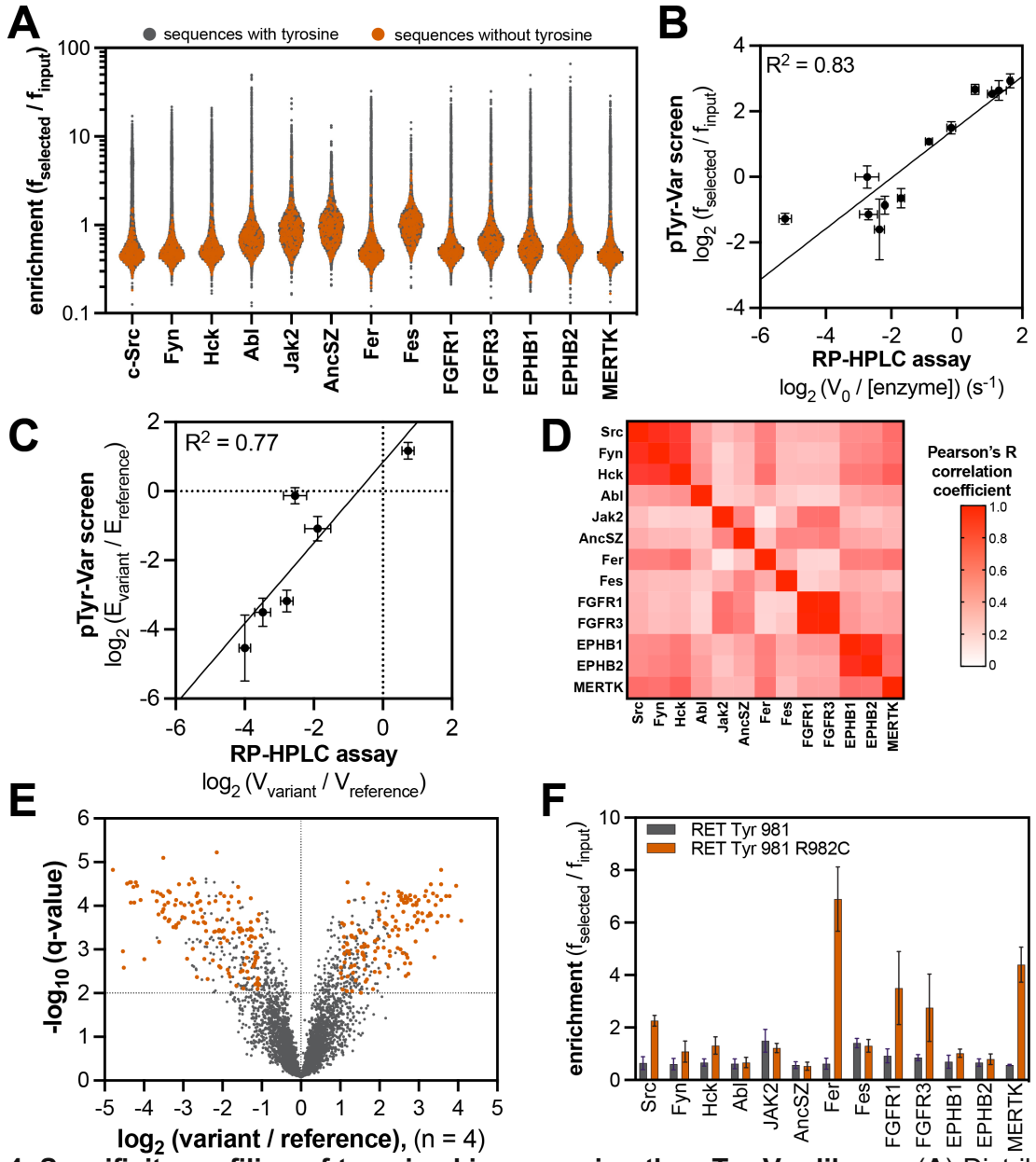

Figure 4. Specificity profiling of tyrosine kinases using the pTyr-Var library. (**A**) Distribution of enrichment scores from pTyr-Var screens with 13 tyrosine kinases. Each point represents a peptide sequence in the pTyr-Var library. Data points in orange-red represent sequences without a Tyr residue and data points in dark gray represent sequences with a Tyr residue. Each dataset represents the average of 3-5 replicates. (**B**) Correlation between enrichment scores and measured phosphorylation rates for 12 peptides (100 μM) with c-Src (500 nM). (**C**) Correlation between the magnitude of mutational effects for 6 peptide pairs in the pTyr-Var library with mutational effects measured using an *in vitro* kinetic assay. Error bars in panels **B** and **C** represent the standard deviation from 3-4 rate measurements and four pTyr-Var screens. (**D**) Matrix of Pearson's correlation coefficients for all pairwise comparisons between replicate-averaged pTyr-Var datasets for 13 kinases. (**E**) Volcano plot depicting mutational effects in the pTyr-Var screen with c-Src kinase domain. Data points represent the average of four replicates. Hits are colored orange-red. (**F**) Enrichment scores from pTyr-Var screens for phosphorylation of the RET Tyr 981 reference and variant (R982C) peptides by 13 tyrosine kinases. Error bars represent the standard deviations from three to five replicates.

For c-Src, we identified 381 high-confidence mutations (Figure 4E). A number of these mutations were on proteins involved in neurotrophin-regulated signaling, cyclin-dependent serine/threonine kinase activity, and other receptor/non-receptor tyrosine kinase activity. We found notable mutational effects at a known target of c-Src, Tyr 149 of the tumor suppressor protein FHL1 (Wang et al., 2018), as well as on other proteins known to interact with c-Src, such as the lipid and protein phosphatase PTEN and the immune receptor LIL4RB (Kang et al., 2016; Lu et al., 2003). We were particularly interested in cases where a kinase not previously known to phosphorylate a specific phosphosite showed a dramatic gain-of-function upon phosphosite-proximal mutation. For example, we found that the R982C mutation, proximal to Tyr 981 on the receptor tyrosine kinase RET, significantly enhanced phosphorylation by c-Src (Figure 4F). This phosphosite is a known to engage the SH2 domain of c-Src and facilitate c-Src activation upon recruitment to RET, but it is not considered a kinase substrate of c-Src (Encinas et al., 2004). This mutation could potentially rewire signaling by promoting phosphorylation of RET by c-Src, and in doing so, sustaining c-Src activation by its binding to phospho-RET. The RET R982C mutation also enhanced Tyr 981 phosphorylation by several other kinases, most notably Fer (Figure 4F). These examples show how the pTyr-Var data could be used as a resource to guide mutation-focused signaling studies.

Phosphosite-proximal mutations can have context-dependent effects on tyrosine kinase recognition.

As noted above, we hypothesized that some mutational effects in our screen might be context-dependent. The same substitution could have different effects depending on the composition of the surrounding sequence. This phenomenon would be uniquely visible in our screening approach, as we are measuring the phosphorylation of defined peptide sequences, and we are conducting screens with thousands of peptide pairs that vary by only a single amino acid substitution. To test our hypothesis, we assessed whether the directionality of mutational effects observed for specific peptides in the pTyr-Var screen could be predicted using the position-specific scoring matrix derived from the X_5-Y-X_5 screen (which would represent the effect of making a substitution averaged over all sequence contexts). While the directionality of the effect of most mutations could be predicted by the X_5-Y-X_5 screen, we observed many mutations that showed a significant effect where none was predicted, as well as mutations where the effect was the opposite of what was predicted (Figure 5A and Figure 5-supplement 1).

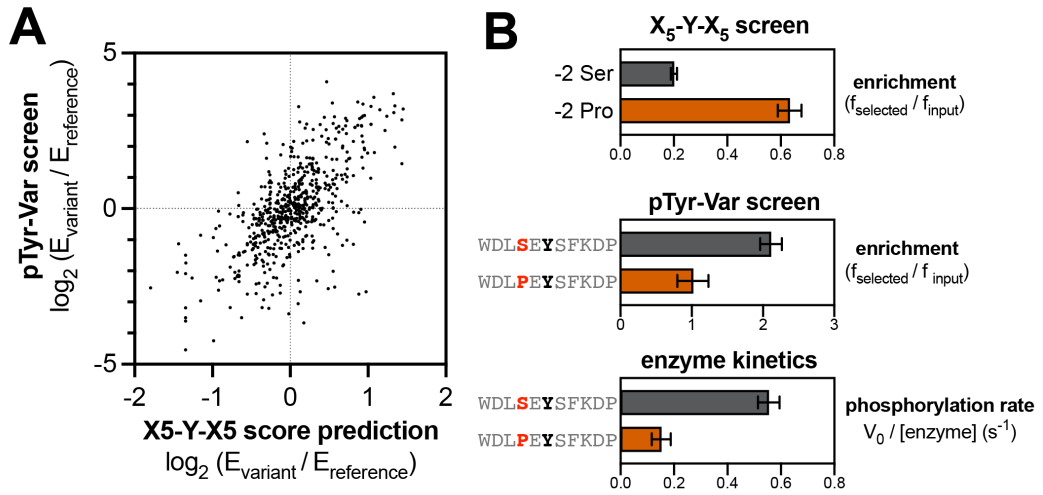

Figure 5. Context-dependent effects of phosphosite-proximal mutations. (**A**) Correlation of variant effects measured in the pTyr-Var library screen with those predicted from the X_5-Y-X_5 library screen for c-Src. Several points lie in the top-left and bottom-right quadrants, indicating a discrepancy between the measured mutational effect in the pTyr-Var screen and the predicted mutational effect from the X_5-Y-X_5 screen. (**B**) Effects of serine-to-proline substitution at the -2 position in various assays with c-Src. The top panel shows the enrichment levels of -2 serine and proline in the X_5-Y-X_5 screen. The middle panel shows the effect of a -2 serine to proline substitution in a specific peptide in the pTyr-Var screen. The bottom panel shows rate measurements using the RP-HPLC assay for the same peptide pair shown in the middle panel.

To validate this observation, we selected a peptide pair in the pTyr-Var library where a mutation (-2 Ser to Pro) had the opposite effect of that predicted by our X_5-Y-X_5 screen for c-Src (Figure 1B), as well as published results with oriented peptide libraries (Begley et al., 2015; Obenauer et al., 2003). We measured rates of phosphorylation of the purified peptides by c-Src using our HPLC assay, which confirmed the result from the pTyr-Var screen and contradicted the X_5-Y-X_5 prediction (Figure 5B). A previous study that analyzed the specificity of the epidermal growth factor receptor (EGFR) kinase using bacterial peptide display showed that the effect of mutations at the -2 position was sometimes dependent on the identity of the -1 residue (Cantor et al., 2018). Molecular dynamics analyses in that report suggested that the amino acid identity at the -1 position determined how the side chain of the -2 residue was presented to the kinase, and vice versa, thereby dictating context-dependent preferences at both positions. Our pTyr-Var screens suggest that context dependent sequence preferences may be commonplace. Depending on the kinase, 5-15% of all significant mutations in the pTyr-Var screen had the opposite effect of that predicted using the X_5-Y-X_5 library data. Mapping these context-dependent effects comprehensively could have a significant impact on our ability to predict native substrates of kinases, and it will improve our understanding of the structural basis for substrate specificity.

Phosphorylation of bacterial peptide display libraries enables profiling of SH2 domains.

In previous implementations of our bacterial peptide display and deep sequencing approach, the specificities of phosphotyrosine recognition domains (e.g. SH2 domains and phosphotyrosine binding (PTB) domains) were analyzed in addition to tyrosine kinase domains (Cantor et al., 2018; Lo et al., 2019). This approach required two amendments to the kinase screening protocol. First, the surface-displayed libraries were phosphorylated to saturating levels using a cocktail of tyrosine kinases. Second, because phosphotyrosine recognition domains generally have fast dissociation rates from their ligands (Morimatsu et al., 2007; Oh et al., 2012), making binding-based selection assays challenging, constructs were generated in which two identical copies of an SH2 domain were artificially fused together. The tandem-SH2 constructs enhanced avidity for phosphopeptides displayed on the cell surface through multivalent effects, thereby enabling enrichment of cells via FACS (Cantor et al., 2018).

For this study, we reasoned that a multivalent SH2 construct could be mimicked by functionalizing avidin-coated magnetic beads with biotinylated SH2 domains. These SH2-coated beads could then be used to select *E. coli* cells displaying enzymatically phosphorylated peptide display libraries, followed by deep sequencing to determine SH2 sequence preferences (Figure 6A). Thus, we first established a protocol to produce site-specifically biotinylated SH2 domains in *E. coli*, by co-expressing an Avi-tagged SH2 construct with the biotin ligase BirA (Gräslund et al., 2017). This system yielded quantitatively biotinylated SH2 domains, as confirmed by mass spectrometry (Figure 6-figure supplement 1). Since the biotinylated SH2 domains could be produced in high yields through bacterial expression, the recognition domains were immobilized on the magnetic beads at saturating concentrations to ensure a uniform concentration across experiments. This also prevented background binding of strep-tagged libraries to the beads, making this method compatible with previously reported strep-tagged libraries (Cantor et al., 2018; Shah et al., 2018, 2016).

To implement SH2 specificity screens, the strep-tagged X_5-Y-X_5 library was phosphorylated to a high level using a mixture of c-Src, c-Abl, AncSZ, and EPHB1 (Figure 6-figure supplement 2). The phosphorylated library was screened against three SH2 domains that fall into distinct specificity classes and are derived from three different types of signaling proteins: the SH2 domain from the tyrosine kinase c-Src, the C-terminal SH2 (C-SH2) domain from the tyrosine phosphatase SHP2, and the SH2 domain from the non-catalytic adaptor protein Grb2 (Figure 6B and Figure 6-source data 1). The X_5-Y-X_5 library screens recapitulated known sequences preferences for each SH2 domain. For c-Src, there was a distinctive preference for -2 His, +1 Asp/Glu, and +3 Ile, as previously reported from oriented peptide libraries (Huang et al., 2008). For Grb2, a characteristic +2 Asn preference dominated the specificity profile (Gram et al., 1997; Huang et al., 2008; Kessels et al., 2002; Rahuel et al., 1996; Songyang et al., 1994b). Notably, our Grb2 screen also reveals subtle amino acid preferences at other positions, which could tune the affinity for +2 Asn-containing sequences. Several studies have measured the sequence

specificity of the SHP2 C-SH2 domain using diverse methods, including peptide microarrays, oriented peptide libraries, and one-bead-on-peptide libraries (Huang et al., 2008; Miller et al., 2008; Sweeney et al., 2005; Tinti et al., 2013). The results of these reported screens are not concordant. Our method

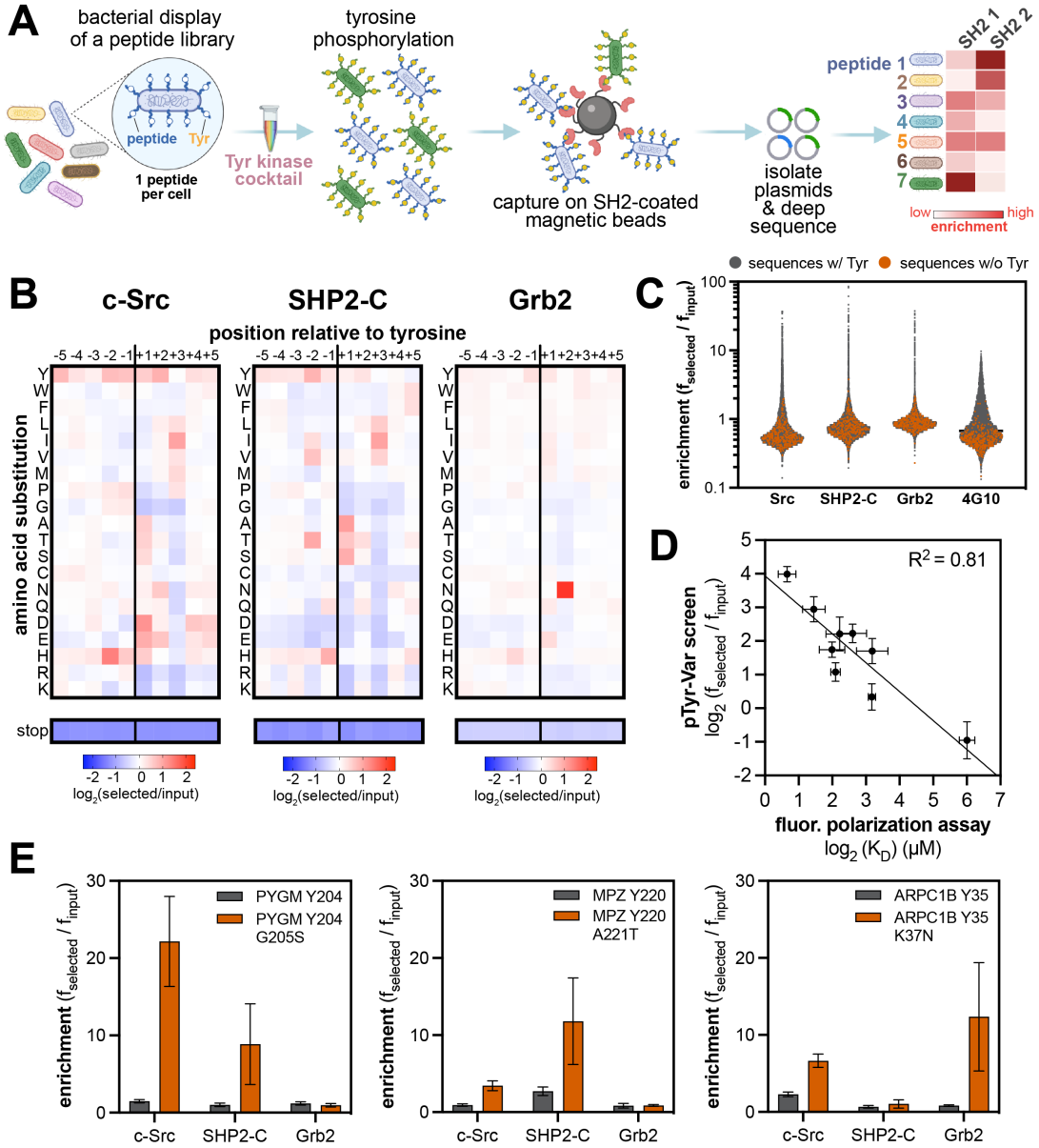

Figure 6. High-throughput profiling of SH2 domain ligand specificity using bacterial peptide display. (**A**) Schematic representation of the workflow for SH2 domain specificity profiling. (**B**) Heatmaps depicting the specificities of the c-Src, SHP2-C, and Grb2 SH2 domains, measured using the X_5-Y-X_5 library. Enrichment scores were $\log_2$-transformed and are displayed on a color scale from blue (disfavored), to white (neutral), to red (favored). Values in the heatmaps are the average of three replicates. (**C**) Distribution of enrichment scores from pTyr-Var screens with three SH2 domains and the pan-phosphotyrosine antibody 4G10 Platinum. Each point represents a peptide sequence in the library. The antibody selection was done similar to the kinase screens, with antibody labeling of cells, followed by bead-based enrichment, as opposed to cell enrichment with antibody-saturated beads. Each dataset represents the average of three replicates. (**D**) Correlation between enrichment scores for 9 peptides from the pTyr-Var screen and binding affinities measured using a fluorescence polarization assay. Error bars represent the standard deviations from three screens or binding measurements. (**E**) Examples of phosphosite-proximal mutations that selectively enhance binding to specific SH2 domains. Error bars represent the standard deviations from three screens.

indicates a preference for β-branched amino acids (Thr/Val/Ile) at the -2 position, a small residue (Ala/Ser/Thr) at the +1 position, and strong preference for an aliphatic residue (Ile/Val/Leu) at the +3 position. Our results are most in-line with the one-bead-one-peptide screens (Sweeney et al., 2005).

We next phosphorylated and screened the pTyr-Var library against the same three SH2 domains in triplicate (Figure 6C and Figure 6-source data 2). The replicates for each SH2 domain were highly correlated, but datasets between SH2 domains had poor correlation, suggesting distinct ligand specificities (Figure 6-figure supplement 3). As observed for kinases, we saw negligible enrichment of peptides lacking a tyrosine residue, but each SH2 domain showed strong enrichment of a few hundred peptides containing one or more tyrosines (Figure 6C). With the phosphorylated pTyr-Var library, we also carried out selection with a biotinylated pan-phosphotyrosine antibody to assess the level of bias in phosphorylation across the library. Compared to selection with SH2 domains, selection with the antibody yielded a narrower distribution of enrichment scores, with very few highly enriched sequences, suggesting relatively uniform phosphorylation (Figure 6C). We further validated the SH2 screening method by measuring the binding affinities of 9 peptides from the pTyr-Var library with the c-Src SH2 domain, using a fluorescence polarization binding assay. Enrichment scores from the pTyr-Var screen showed a good linear correlation with measured K_d values over two orders of magnitude (Figure 6D).

The pTyr-Var library screens with the SH2 domains were analyzed and filtered similarly to those with kinase domains. For each SH2 domain, we identified a 50-300 phosphosite-proximal mutations that significantly and reproducibly enhanced or attenuated binding (Figure 6-figure supplement 4 and Figure 6-source data 2). As expected, given their distinct specificities, the c-Src, SHP2-C, and Grb2 SH2 domains showed unique sensitivities to mutations (Figure 6-figure supplement 5). We identified several phosphosite-proximal mutations that were selectively gain-of-function for one or two SH2 domains (Figure 6E and Figure 6-source data 2). These mutations could drive the rewiring of signaling pathways by changing which downstream effector engages a phosphosite. This phenomenon was recently reported for lung-cancer associated mutations near phosphorylation sites in EGFR, which impacted the recruitment of Grb2 and SHP2 to the receptor and altered downstream signaling (Lundby et al., 2019).

Finally, we note that our pTyr-Var datasets included screens with both the kinase and SH2 domains of c-Src. When the SH2 domain of c-Src interacts with phosphoproteins, it both localizes the kinase domain in proximity to its substrates and activates the enzyme (Liu et al., 1993). Our screens revealed that the phosphorylation profiles of c-Src kinase and SH2 domains against the pTyr-Var were completely orthogonal (Figure 6-figure supplement 6). Notably, mutations that impacted one domain generally had no effect on the other, because preferred sequence features for one domain were typically tolerated (neutral) for the other (Figure 6-figure supplement 7). A consequence of this is that phosphosite-proximal mutations may alter c-Src function in two mechanistically distinct ways: (1) mutations that enhance SH2 binding can alter the localization and local activation of c-Src, or (2) mutations that enhance kinase recognition will directly increase phosphorylation rates by c-Src. These insights highlight value in profiling multiple domains of the same signaling protein against the same peptide library.

Amber codon suppression yields an expanded repertoire of peptides for specificity profiling.

The specificity profiling screens described thus far were constrained to sequences that contain the canonical twenty amino acids. Several studies have suggested that non-canonical amino acids and post-translationally modified amino acids can also impact sequence recognition by tyrosine kinases and SH2 domains (Alfaro-Lopez et al., 1998; Begley et al., 2015; Chapelat et al., 2012; Johnson et al., 2022; Yeh et al., 2001). The most notable example of this is phospho-priming, whereby phosphorylation of one residue on a protein enhances the ability of a kinase to recognize and phosphorylate a proximal residue. This phenomenon was recently described for EGFR, which preferentially phosphorylates sequences containing a tyrosine followed by a +1 phosphotyrosine (Begley et al., 2015). Other prevalent post-translational modifications, such as lysine acetylation, may also impact the ability of kinases or SH2 domains to recognize a particular phosphosite (Parker et al., 2014; Rust and Thompson, 2011).

We sought to expand our specificity profiling method to incorporate non-canonical and post-

translationally modified amino acids (Figure 7A). Since our libraries are genetically encoded, we employed Amber codon suppression and repurposing, using engineered tRNA molecules and aminoacyl tRNA synthetases (Amiram et al., 2015; Xie et al., 2007; Zheng et al., 2018). The degenerate (X)

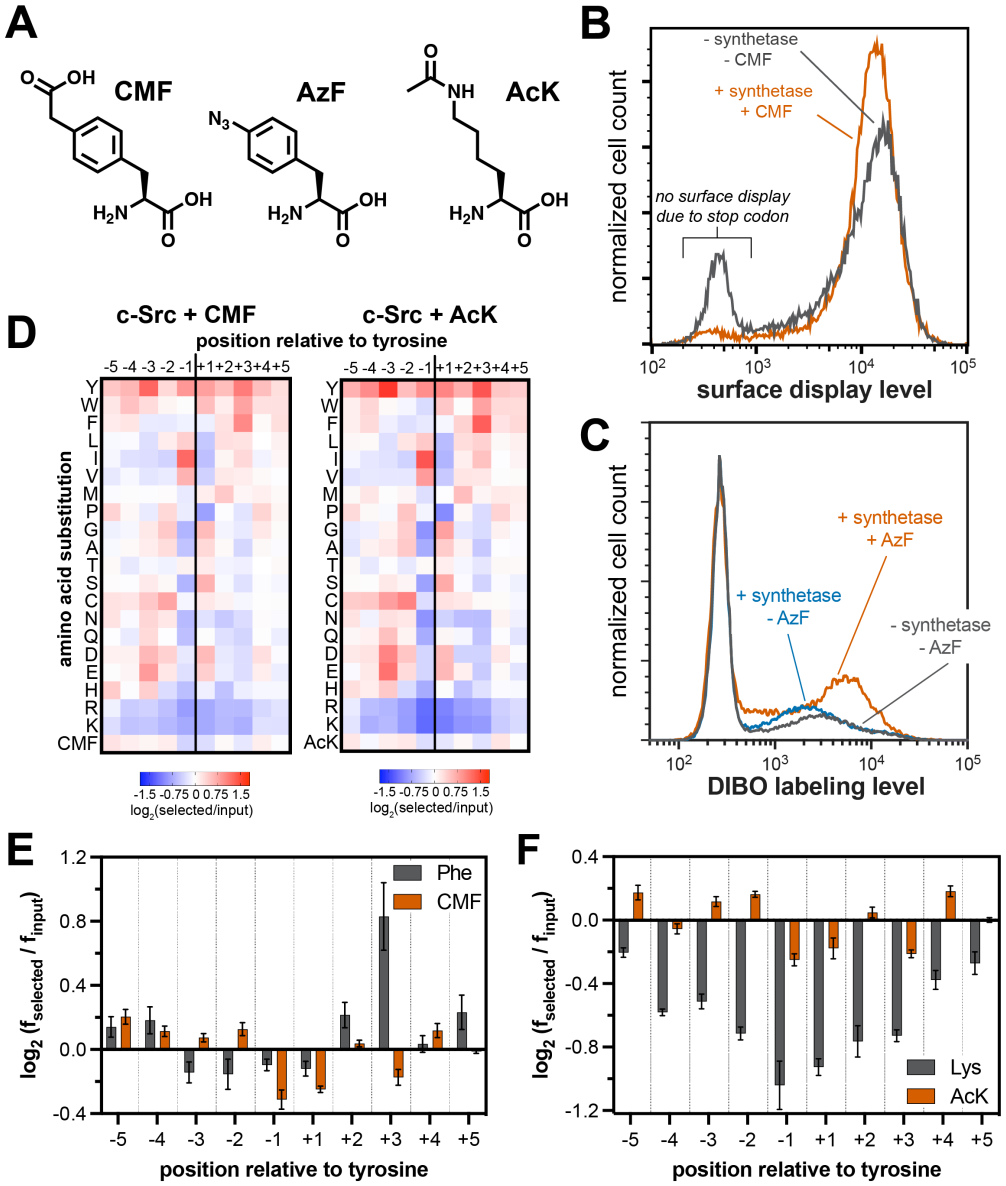

Figure 7. Expansion of peptide display libraries using Amber suppression. (**A**) Non-canonical amino acids used in this study. CMF = 4-carboxymethyl phenylalanine, AzF = 4-azido phenylalanine, and AcK = N-ε-acetyl-L-lysine. (**B**) Amber suppression in the strep-tagged X_5-Y-X_5 library using CMF. Library surface-display level was monitored by flow cytometry using a fluorophore-labeled StrepMAB antibody for samples with or without Amber suppression components. (**C**) AzF labeling on bacterial cells using a DIBO-conjugated fluorophore. Cells expressing the X_5-Y-X_5 library, with and without various Amber suppression components, were treated with DIBO-conjugated Alexa Fluor 555 then analyzed by flow cytometry. (**D**) Heatmaps depicting the specificities of c-Src after CMF and acetyl lysine incorporation. Only sequences with one stop codon were used in this analysis. Enrichment scores were $\log_2$-transformed and are displayed on a color scale from blue (disfavored), to white (neutral), to red (favored). Values in heatmaps are the average of three replicates. (**E**) Comparison of the enrichment values for phenylalanine (Phe) and CMF at each position surrounding the central tyrosine in the c-Src kinase X_5-Y-X_5 screens. (**F**) Comparison of the enrichment values for lysine (Lys) and acetyl-lysine (AcK) at each position surrounding the central tyrosine in the c-Src kinase X_5-Y-X_5 screens. Error bars in panels **E** and **F** represent the standard deviations from three screens.

positions in our X_5-Y-X_5 library are encoded using an NNS codon, which means that an Amber codon (TAG) is sampled at each position 3% of the time. Thus, this library theoretically contains a sufficiently large number of diverse sequences to profile specificity with a 21 amino acid alphabet. For Amber suppression in *E. coli*, tRNA/synthetase pairs are commonly expressed from pEVOL or pULTRA plasmids (chloramphenicol and streptomycin resistant, respectively) (Chatterjee et al., 2013). Both of these systems are incompatible with our surface-display platform, which uses MC1061 cells (streptomycin resistance encoded in the genome) and libraries in a pBAD33 vector (chloramphenicol resistant). Thus, we designed a variant of the pULTRA plasmid in which we swapped the streptomycin resistance gene for an ampicillin resistance gene from a common pET vector for protein expression (pULTRA-Amp).

To confirm that non-canonical amino acids could be incorporated into the X_5-Y-X_5 library, we co-transformed *E. coli* with the library and a pULTRA-Amp plasmid encoding a tRNA/synthetase pair that can incorporate the phosphotyrosine analog 4-carboxymethyl phenylalanine (CMF) via Amber suppression (Figure 7A) (Xie et al., 2007). We measured peptide display levels by flow cytometry for cultures that were grown with or without CMF in the media. For the cultures grown without CMF, roughly 20% of the cells had no surface-displayed peptides, consistent with termination of translation at Amber codons within the peptide-coding region (Figure 7B). In the presence of CMF, this premature termination was significantly suppressed, and a larger fraction of the cells displayed peptides. As an additional test, we encoded 4-azido phenylalanine (AzF) into the X_5-Y-X_5 library (Figure 7A) (Amiram et al., 2015). Cells expressing this expanded library were treated with a dibenzocyclooctyne-functionalized fluorophore, which should selectively react with the azide on AzF via strain-promoted azide-alkyne cycloaddition (Ning et al., 2008). Only cells expressing the synthetase and grown in the presence of AzF showed significant DIBO labeling, confirming Amber suppression and non-canonical amino acid incorporation into our library (Figure 7C).

Using this library expansion strategy, we assessed how substrate recognition by the c-Src kinase domain is impacted by neighboring CMF or acetyl-lysine residues. We subjected CMF- and AcK-containing X_5-Y-X_5 libraries to c-Src phosphorylation, selection, and sequencing, using the same methods described above. When analyzing X_5-Y-X_5 libraries in standard kinase and SH2 screens, we typically omit all Amber-containing sequences from our calculations, as they do not encode expressed peptides (Figures 1B and 2A). For these experiments, we included Amber-containing sequences in our analysis. Using this strategy, we found that the Amber codon was less depleted at each position surrounding the central tyrosine than we observed for libraries without Amber suppression, but the log-transformed enrichment scores for Amber codons at all positions surrounding the tyrosine residue were still negative (Figure 7-figure supplement 1). We reasoned that, if Amber suppression efficiency was not 100%, any Amber-containing sequence would still be depleted relative to a sequencing lacking a stop codon, due to some premature termination. Thus, we re-analyzed the data by exclusively counting sequences that contained one Amber codon, under the assumption that every sequence would have approximately the same amount of premature termination. This revealed positive enrichment for CMF and AcK at select positions (Figure 7D-F). Although we only included a fraction of the total library in our new analysis, the overall specificity profile was almost identical to that observed when including the whole library, indicating that this sub-sampling approach was valid (Figure 7D and Figure 7-figure supplement 2).

Finally, we compared the preferences for CMF and AcK at each position to their closest canonical amino acids, phenylalanine (Phe) and lysine (Lys). CMF was enriched at the -3 and -2 positions, where Phe is not tolerated by c-Src (Figure 7E). Negatively-charged amino acids (Asp and Glu) are also preferred at these positions, and the negative charge on the carboxymethyl group of CMF at neutral pH may be able to mimic this recognition. c-Src has a strong selective preference for Phe at the +3 position, which it engages via a well-formed hydrophobic pocket near the active site (Bose et al., 2006; Shah et al., 2018). The charged carboxymethyl group on CMF is likely to be incompatible with this mode of binding, consistent with depletion of CMF at this site (Figure 7E). The difference between Lys and AcK was even more striking. Lys is unfavorable for c-Src at every position around the phospho-acceptor tyrosine. By contrast, AcK was not only tolerated, but even favorable at a few positions (Figure 7F). This pattern of acetyl-lysine preference over lysine could be used to predict sites in the proteome where lysine acetylation creates a new, high-activity substrate for c-Src. Furthermore, the same analysis could be

applied to other tyrosine kinases and to SH2 domains, and our strategy could be readily expanded to other post-translational modifications that can be encoded using Amber suppression.

Concluding remarks

In this report, we describe a significant expansion to a previously developed method for profiling the sequence specificities of tyrosine kinases and SH2 (phosphotyrosine recognition) domains (Cantor et al., 2018; Shah et al., 2018, 2016). Our method relies on bacterial display of DNA-encoded peptide libraries and deep sequencing, and it enables the simultaneous analysis of multiple phosphotyrosine signaling proteins against thousands-to-millions of peptides or phosphopeptides. The resulting data can be used to design high-activity consensus sequences, predict the activities of uncharacterized sequences, and accurately measure the effects of amino acid substitutions on sequence recognition. A notable feature of our platform is that it relies on deep sequencing as a readout, yielding highly quantitative results. Furthermore, the data generated from our screens show a strong correlation with phosphorylation rates and binding affinities measured using orthogonal biochemical assays.

We envision a number of exciting applications of this expanded specificity profiling platform. Several recent reports have aimed to explain the molecular basis for tyrosine kinase and SH2 sequence specificity and affinity, by combining protein sequence and structure analysis with specificity profiling data (Bradley et al., 2021; Creixell et al., 2015a; Kaneko et al., 2010; Liu et al., 2019). The rich datasets generated using our platform will augment these approaches, particularly when coupled with screening data for additional proteins. A long-term goal of these efforts will undoubtedly be to accurately predict the sequence specificity and signaling properties of any uncharacterized phosphotyrosine signaling protein, such as a disease-associated kinase variant (Creixell et al., 2015b). Given the nature of the data generated by our platform, we expect that it will also aid the development and implementation of machine learning models for sequence specificity and design (Creixell et al., 2015a; Cunningham et al., 2020; Kundu et al., 2013). Indeed, our initial efforts in this realm suggest that specificity profiling data using the X_5-Y-X_5 library, without any protein structural information, may be sufficient to build models of sequence specificity that can accurately predict phosphorylation rates (Rube et al., 2022).

The pTyr-Var Library described in this report provides a unique opportunity to investigate variant effects across the human proteome. The vast majority of mutations near tyrosine phosphorylation sites are functionally uncharacterized (Hornbeck et al., 2019; Krassowski et al., 2018). Our screens are yielding some of the first mechanistic biochemical hypotheses about how many of these mutations could impact cell signaling. For example, these datasets will allow us to identify mutations that tune signaling pathways by altering the phosphorylation efficiency of specific phosphosites or the binding of SH2-containing effector proteins to those sites. Alternatively, these screens may help identify instances of network rewiring, in which a phosphosite-proximal mutation alters the canonical topology of a pathway by changing which kinases phosphorylate a phosphosite or which SH2-containing proteins get recruited to that site. The biological effects of signal tuning and rewiring caused by phosphosite-proximal mutations remain largely unexplored.

Our high-throughput platform to profile tyrosine kinase and SH2 sequence recognition is accessible and easy to use in labs that are equipped to culture *E. coli* and execute common molecular biology and biochemistry techniques. Screens can be conducted on the benchtop with proteins produced in-house or obtained from commercial vendors. Peptide libraries of virtually any composition, tailored to address specific biochemical questions, can be produced using commercially available oligonucleotides and standard molecular cloning techniques. Furthermore, facile chemical changes to the library (e.g. enzymatic phosphorylation or the introduction of non-canonical amino acids via Amber suppression) afford access to new biochemical questions. For example, the tyrosine-phosphorylated libraries described here will also be useful for the characterization of tyrosine phosphatase specificity, and acetyl-lysine-containing libraries could be used to profile lysine deacetylases and bromodomains. Additional amendments to this platform will enable the analysis of serine/threonine kinases and other protein modification or recognition domains, adding to the growing arsenal of robust methods for the high-throughput biochemical characterization of cell signaling proteins.

Materials and methods

Key resources table

Reagent type (species) or resource	Designation	Source or reference	Identifiers	Additional information
strain, strain background (*E. coli*)	MC1061	Lucigen	Lucigen: 10361012	bacterial cells used for surface-display screens
strain, strain background (*E. coli*)	DH5α	Invitrogen	Invitrogen: 18265017	bacterial cells used for general cloning and library cloning
strain, strain background (*E. coli*)	BL21(DE3)	ThermoFisher Scientific	Thermo: C600003	bacterial cells for general protein-expression; pre-transformed with pCDF-YopH for tyrosine kinase overexpression
strain, strain background (*E. coli*)	C43(DE3)	Lucigen	Lucigen: NC9581214	bacterial cells used for SH2 domain over-expression; pre-transformed with pCDFDuet-BirA-WT for biotinylation
antibody	4G10™ Platinum, Biotin	Millipore Sigma	Millipore Sigma: 16-452-MI	biotin conjugated mouse monoclonal pan-phosphotyrosine antibody (1:1000 dilution)
antibody	PY20-PerCP-eFluor 710	eBioscience	eBioscience: 46-5001-42	PerCP-eFluor 710-conjugated mouse monoclonal pan-phosphotyrosine antibody, clone PY20 (1:25 dilution)
antibody	PY20-biotin	Exalpha	Exalpha: 50-210-1865	biotin conjugated mouse monoclonal pan-phosphotyrosine antibody (1:500 dilution)
antibody	StrepMAB Chromeo 488	IBA LifeSciences	IBA: 2-1546-050	Chromeo 488-conjugated antibody that recognizes the strep-tag (1:50-1:100 dilution). Discontinued, but can be replaced with IBA LifeSciences StrepMAB-Classic conjugate DY-488 (IBA: 2-1563-050)
recombinant DNA reagent	pBAD33-eCPX	PMID: 18480093	Addgene: 23336	pBAD33 plasmid encoding the eCPX bacterial display gene with flanking 5' and 3' SfiI restriction sites
recombinant DNA reagent	pBAD33-eCPX-cStrep	PMID: 29547119		pBAD33 plasmid encoding the eCPX bacterial display gene with a 3' sequence encoding a strep-tag and flanking 5' and 3' SfiI restriction sites
recombinant DNA reagent	pBAD33-eCPX-cMyc	this paper		pBAD33 plasmid encoding the eCPX bacterial display gene with a 3' sequence encoding a myc-tag and flanking 5' and 3' SfiI restriction sites
recombinant DNA reagent	X5-Y-X5 Library (myc-tagged)	this paper		peptide display library in the pBAD33 vector, fused to the eCPX scaffold, containing 1-10 million unique sequences with the structure X5-Y-X5, where X is encoded by an NNS codon. The scaffold protein is encoded to have a C-terminal myc-tag: EQKLISEEDL.
recombinant DNA reagent	X5-Y-X5 Library (strep-tagged)	this paper		peptide display library in the pBAD33 vector, fused to the eCPX scaffold, containing 1-10 million unique sequences with the structure X5-Y-X5, where X is encoded by an NNS codon. The scaffold protein is encoded to have a C-terminal strep-tag: WSHPQFEK.
recombinant DNA reagent	pTyr-Var Library (myc-tagged)	this paper		peptide display library in the pBAD33 vector, fused to the eCPX scaffold, containing ~10,000 unique sequences encoding reference and variant phosphosite pairs deried from the PhosphoSitePlus database. The scaffold protein is encoded to have a C-terminal myc-tag: EQKLISEEDL.
recombinant DNA reagent	pTyr-Var Library (strep-tagged)	this paper		peptide display library in the pBAD33 vector, fused to the eCPX scaffold, containing ~10,000 unique sequences encoding reference and variant phosphosite pairs deried from the PhosphoSitePlus database. The scaffold protein is

				encoded to have a C-terminal strep-tag: WSHPQFEK.
recombinant DNA reagent	pET-23a-His6-TEV-Src(KD)	PMID: 29547119		bacterial expression vector encoding the human c-Src kinase domain (residues 260-528), with an N-terminal His6-tag and TEV protease recognition sequence
recombinant DNA reagent	pET-23a-His6-TEV-Fyn(KD)	PMID: 29547119		bacterial expression vector encoding the human Fyn kinase domain (residues 261–529) with an N-terminal His6-tag and TEV protease recognition sequence
recombinant DNA reagent	pET-23a-His6-TEV-Hck(KD)	PMID: 29547119		bacterial expression vector encoding the human Hck kinase domain (residues 252–520) with an N-terminal His6-tag and TEV protease recognition sequence
recombinant DNA reagent	pET-23a-His6-TEV-Abl(KD)	PMID: 29547119		bacterial expression vector encoding the mouse c-Abl kinase domain (residues 232–502) with an N-terminal His6-tag and TEV protease recognition sequence
recombinant DNA reagent	pET-23a-His6-TEV-AncSZ(KD)	DOI 10.1101/2022.04.24.489292		bacterial expression vector encoding the AncSZ kinase domain (residues 352-627) with an N-terminal His6-tag and TEV protease recognition sequence
recombinant DNA reagent	pET23a-His6-TEV-Fer(KD)	this paper		bacterial expression vector encoding the mouse Fer kinase domain (residues 553-823) with an N-terminal His6-tag and TEV protease recognition sequence
recombinant DNA reagent	pET-His6-TEV-Fes(KD)	PMID: 30004690	Addgene: 79686	bacterial expression vector encoding the human Fes kinase domain (residues 551-822) with an N-terminal His6-tag and TEV protease recognition sequence
recombinant DNA reagent	pET-His6-TEV-FGFR1(KD)	PMID: 30004690	Addgene: 79719	bacterial expression vector encoding the human FGFR1 kinase domain (residues 456-763) with an N-terminal His6-tag and TEV protease recognition sequence
recombinant DNA reagent	pET-His6-TEV-FGFR3(KD)	PMID: 30004690	Addgene: 79731	bacterial expression vector encoding the human FGFR3 kinase domain (residues 449-759) with an N-terminal His6-tag and TEV protease recognition sequence
recombinant DNA reagent	pET-His6-TEV-EPHB1(KD)	PMID: 30004690	Addgene: 79694	bacterial expression vector encoding the human EPHB1 kinase domain (residues 602-896) with an N-terminal His6-tag and TEV protease recognition sequence
recombinant DNA reagent	pET-His6-TEV-EPHB2(KD)	PMID: 30004690	Addgene: 79697	bacterial expression vector encoding the human EPHB2 kinase domain (residues 604-898) with an N-terminal His6-tag and TEV protease recognition sequence
recombinant DNA reagent	pET-His6-TEV-MERTK(KD)	PMID: 30004690	Addgene: 79705	bacterial expression vector encoding the human MERTK kinase domain (residues 570-864) with an N-terminal His6-tag and TEV protease recognition sequence
recombinant DNA reagent	pCDF-YopH	PMID: 16260764		bacterial expression vector for co-expression of untagged YopH phosphatase with tyrosine kinases
recombinant DNA reagent	pCDFDuet-BirA-WT	this paper		bacterial expression vector encoding BirA biotin ligase, used to coexpress with SH2 domain expression vector for biotinylation of SH2 domain
recombinant DNA reagent	pET-His6-SUMO-Src(SH2)	this paper		bacterial expression vector encoding the human cSrc SH2 domain (residues 143-250) with an N-terminal His6-SUMO tag
recombinant DNA reagent	pET-His6-SUMO-SHP2(CSH2)	this paper		bacterial expression vector encoding the human SHP2 CSH2 domain (residues 105-220) with an N-terminal His6-SUMO tag

recombinant DNA reagent	pET-His6-SUMO-Grb2(SH2)	this paper		bacterial expression vector encoding the human Grb2 SH2 domain (residues 56-152) with an N-terminal His6-SUMO tag
recombinant DNA reagent	pULTRA CMF	PMID: 28604693		bacterial expression vector encoding the tRNA/syntetase pair for incorporation of 4-carboxymethyl phenylalanine via Amber suppression
recombinant DNA reagent	pEVOL pAzFRS.2.t1	PMID: 26571098	Addgene: 73546	bacterial expression vector encoding the tRNA/syntetase pair for incorporation of 4-azido phenylalanine and other Phe derivatives via Amber suppression
recombinant DNA reagent	pULTRA chAcKRS3	PMID: 29544052		bacterial expression vector encoding the tRNA/syntetase pair for incorporation of acetyl-lysine via Amber suppression; gift from Abhishek Chatterjee at Boston College
recombinant DNA reagent	pULTRA-Amp CMF	this paper		bacterial expression vector encoding the tRNA/syntetase pair for incorporation of 4-carboxymethyl phenylalanine via Amber suppression, altered to have an ampicillin resistance marker
recombinant DNA reagent	pULTRA-Amp pAzFRS.2.t1	this paper		bacterial expression vector encoding the tRNA/syntetase pair for incorporation of 4-azido phenylalanine and other Phe derivatives via Amber suppression, altered to have an ampicillin resistance marker
recombinant DNA reagent	pULTRA-Amp chAcKRS3	this paper		bacterial expression vector encoding the tRNA/syntetase pair for incorporation of acetyl-lysine via Amber suppression, altered to have an ampicillin resistance marker
sequence-based reagent	X5-Y-X5 library oligo; eCPX-rand-lib	this paper, purchased from Millipore Sigma		primer sequence: 5'-GCTGGCCAGTCTGGCCAGNNSNNSNNSNNSNNStatNNSNNSNNSNNSNNSGGAGGGCAGTCTGGGCAGTCTG 3'
sequence-based reagent	Oligopool-fwd-primer	this paper, purchased from Millipore Sigma		primer sequence: 5'-GCTGGCCAGTCTG-3'
sequence-based reagent	Oligopool-rev-primer	this paper, purchased from Millipore Sigma		primer sequence: 5'-CAGACTGCCCAGACT-3'
sequence-based reagent	link-eCPX-fwd	this paper, purchased from Millipore Sigma		5'-GGAGGGCAGTCTGGGCAGTCTG-3'
sequence-based reagent	link-eCPX-rev	this paper, purchased from Millipore Sigma		5'-GCTTGGCCACCTTGGCCTTATTA-3'
sequence-based reagent	BB-fwd-primer	this paper, purchased from Millipore Sigma		5'-TAATAAGGCCAAGGTGGCCAAGC-3'
sequence-based reagent	BB-rev primer	this paper, purchased from Millipore Sigma		5'-CTGGCCAGACTGGCCAGCTACG-3'
sequence-based reagent	TruSeq-eCPX-Fwd	sequence from PMID: 29547119, purchased from Millipore Sigma	round one amplicon PCR primer	primer sequence: 5'-TGACTGGAGTTCAGACGTGTGCTCTTCCGATCTNNNNNNACCGCAGGTACTTCCGTAGCT-3'

sequence-based reagent	TruSeq-eCPX-Rev	sequence from PMID: 29547119, purchased from Millipore Sigma	round one amplicon PCR primer	primer sequence: 5’-CACTCTTTCCCTACACGACGCTCTTCCGATCTNNNNNNTTTTGTTGTAGTCACCAGACTG-3’
sequence-based reagent	D701	sequence from Illumina, purchased from Millipore Sigma	round two amplicon/indexing PCR primer	primer sequence: 5'-CAAGCAGAAGACGGCATACGAGATcgagtaatGTGACTGGAGTTCAGACGTG-3'
sequence-based reagent	D702	sequence from Illumina, purchased from Millipore Sigma	round two amplicon/indexing PCR primer	primer sequence: 5'-CAAGCAGAAGACGGCATACGAGATtctccggaGTGACTGGAGTTCAGACGTG-3'
sequence-based reagent	D703	sequence from Illumina, purchased from Millipore Sigma	round two amplicon/indexing PCR primer	primer sequence: 5'-CAAGCAGAAGACGGCATACGAGATaatgagcgGTGACTGGAGTTCAGACGTG-3'
sequence-based reagent	D704	sequence from Illumina, purchased from Millipore Sigma	round two amplicon/indexing PCR primer	primer sequence: 5'-CAAGCAGAAGACGGCATACGAGATggaatctcGTGACTGGAGTTCAGACGTG-3'
sequence-based reagent	D705	sequence from Illumina, purchased from Millipore Sigma	round two amplicon/indexing PCR primer	primer sequence: 5'-CAAGCAGAAGACGGCATACGAGATttctgaatGTGACTGGAGTTCAGACGTG-3'
sequence-based reagent	D706	sequence from Illumina, purchased from Millipore Sigma	round two amplicon/indexing PCR primer	primer sequence: 5'-CAAGCAGAAGACGGCATACGAGATacgaattcGTGACTGGAGTTCAGACGTG-3'
sequence-based reagent	D707	sequence from Illumina, purchased from Millipore Sigma	round two amplicon/indexing PCR primer	primer sequence: 5'-CAAGCAGAAGACGGCATACGAGATagcttcagGTGACTGGAGTTCAGACGTG-3'
sequence-based reagent	D708	sequence from Illumina, purchased from Millipore Sigma	round two amplicon/indexing PCR primer	primer sequence: 5'-CAAGCAGAAGACGGCATACGAGATgcgcattaGTGACTGGAGTTCAGACGTG-3'
sequence-based reagent	D709	sequence from Illumina, purchased from Millipore Sigma	round two amplicon/indexing PCR primer	primer sequence: 5'-CAAGCAGAAGACGGCATACGAGATcatagccgGTGACTGGAGTTCAGACGTG-3'
sequence-based reagent	D710	sequence from Illumina, purchased from Millipore Sigma	round two amplicon/indexing PCR primer	primer sequence: 5'-CAAGCAGAAGACGGCATACGAGATttcgcggaGTGACTGGAGTTCAGACGTG-3'
sequence-based reagent	D711	sequence from Illumina, purchased from Millipore Sigma	round two amplicon/indexing PCR primer	primer sequence: 5'-CAAGCAGAAGACGGCATACGAGATgcgcgagaGTGACTGGAGTTCAGACGTG-3'
sequence-based reagent	D712	sequence from Illumina, purchased	round two amplicon/indexing PCR primer	primer sequence: 5'-CAAGCAGAAGACGGCATACGAGATctatcgctGTGACTGGAGTTCAGACGTG-3'

		from Millipore Sigma		
sequence-based reagent	D501	sequence from Illumina, purchased from Millipore Sigma	round two amplicon/indexing PCR primer	primer sequence: 5'-AATGATACGGCGACCACCGAGATCTACACtatagcctACACTCTTTCCCTACACGAC-3'
sequence-based reagent	D502	sequence from Illumina, purchased from Millipore Sigma	round two amplicon/indexing PCR primer	primer sequence: 5'-AATGATACGGCGACCACCGAGATCTACACatagaggcACACTCTTTCCCTACACGAC-3'
sequence-based reagent	D503	sequence from Illumina, purchased from Millipore Sigma	round two amplicon/indexing PCR primer	primer sequence: 5'-AATGATACGGCGACCACCGAGATCTACACcctatcctACACTCTTTCCCTACACGAC-3'
sequence-based reagent	D504	sequence from Illumina, purchased from Millipore Sigma	round two amplicon/indexing PCR primer	primer sequence: 5'-AATGATACGGCGACCACCGAGATCTACACggctctgaACACTCTTTCCCTACACGAC-3'
sequence-based reagent	D505	sequence from Illumina, purchased from Millipore Sigma	round two amplicon/indexing PCR primer	primer sequence: 5'-AATGATACGGCGACCACCGAGATCTACACaggcgaagACACTCTTTCCCTACACGAC-3'
sequence-based reagent	D506	sequence from Illumina, purchased from Millipore Sigma	round two amplicon/indexing PCR primer	primer sequence: 5'-AATGATACGGCGACCACCGAGATCTACACtaatcttaACACTCTTTCCCTACACGAC-3'
sequence-based reagent	D507	sequence from Illumina, purchased from Millipore Sigma	round two amplicon/indexing PCR primer	primer sequence: 5'-AATGATACGGCGACCACCGAGATCTACACcaggacgtACACTCTTTCCCTACACGAC-3'
sequence-based reagent	D508	sequence from Illumina, purchased from Millipore Sigma	round two amplicon/indexing PCR primer	primer sequence: 5'-AATGATACGGCGACCACCGAGATCTACACgtactgacACACTCTTTCCCTACACGAC-3'
peptide, recombinant protein	Src(KD)	this paper, expressed/purified in-house		human c-Src kinase domain (residues 260-528)
peptide, recombinant protein	Fyn(KD)	this paper, expressed/purified in-house		human Fyn kinase domain (residues 261–529)
peptide, recombinant protein	Hck(KD)	this paper, expressed/purified in-house		human Hck kinase domain (residues 252–520)
peptide, recombinant protein	Abl(KD)	this paper, expressed/purified in-house		mouse c-Abl kinase domain (residues 232–502)
peptide, recombinant protein	JAK2 Protein, active	Millipore Sigma	Millipore Sigma: 14-640-M	Active, C-terminal His6-tagged, recombinant, human JAK2, amino acids 808-end, expressed by baculovirus in Sf21 cells, for use in Enzyme Assays.
peptide, recombinant protein	AncSZ(KD)	this paper, expressed/purified in-house		AncSZ kinase domain (residues 352-627) designed by ancestral sequence reconstruction
peptide, recombinant protein	Fer(KD)	this paper, expressed/purified in-house		mouse Fer kinase domain (residues 553-823)

peptide, recombinant protein	Fes(KD)	this paper, expressed/purified in-house		human Fes kinase domain (residues 551-822)
peptide, recombinant protein	FGFR1(KD)	this paper, expressed/purified in-house		human FGFR1 kinase domain (residues 456-763)
peptide, recombinant protein	FGFR3(KD)	this paper, expressed/purified in-house		human FGFR3 kinase domain (residues 449-759)
peptide, recombinant protein	EPHB1(KD)	this paper, expressed/purified in-house		human EPHB1 kinase domain (residues 602-896)
peptide, recombinant protein	EPHB2(KD)	this paper, expressed/purified in-house		human EPHB2 kinase domain (residues 604-898)
peptide, recombinant protein	MERTK(KD)	this paper, expressed/purified in-house		human MERTK kinase domain (residues 570-864)
peptide, recombinant protein	Src(SH2)	this paper, expressed/purified in-house		human c-Src SH2 domain (residues 143-250)
peptide, recombinant protein	SHP2(C-SH2)	this paper, expressed/purified in-house		human SHP2 C-SH2 domain (residues 105-220)
peptide, recombinant protein	Grb2(SH2)	this paper, expressed/purified in-house		human Grb2 SH2 domain (residues 56-152)
peptide, recombinant protein	Src Consensus	this paper, synthesized in-house		peptide sequence: Ac-GPDECIYDMFPFKKKG-NH2
peptide, recombinant protein	Src Consensus (P-5C, D+1G)	this paper, synthesized in-house		peptide sequence: Ac-GCDECIYGMFPFRRRG-NH2
peptide, recombinant protein	Abl Consensus	this paper, synthesized in-house		peptide sequence: Ac-GPDEPIYAVPPIKKKG-NH2
peptide, recombinant protein	Fer Consensus	this paper, synthesized in-house		peptide sequence: Ac-GPDEPIYEWWWIKKKG-NH2
peptide, recombinant protein	EPHB1 Consensus	this paper, synthesized in-house		peptide sequence: Ac-GPPEPNYEVIPPKKKG-NH2
peptide, recombinant protein	EPHB2 Consensus	this paper, synthesized in-house		peptide sequence: Ac-GPPEPIYEVPPPKKKG-NH2
peptide, recombinant protein	SrcTide (1995)	sequence from PMID: 7845468, synthesized in-house		peptide sequence: Ac-GAEEEIYGEFEAKKKG-NH2
peptide, recombinant protein	SrcTide (2014)	sequence from PMID: 25164267, purchased from Synpeptide		peptide sequence: Ac-GAEEEIYGIFGAKKKG-NH2
peptide, recombinant protein	AblTide (2014)	sequence from PMID: 7845468, synthesized in-house		peptide sequence: Ac-GAPEVIYATPGAKKKG-NH2
peptide, recombinant protein	HRAS_Y64	sequence from PMID: 35606422,		peptide sequence: Ac-AGQEEYSAMRD-NH2

		purchased from Synpeptide		
peptide, recombinant protein	HRAS_Y64_E63K	sequence from PMID: 35606422, purchased from Synpeptide		peptide sequence: Ac-AGQEKYSAMRD-NH2
peptide, recombinant protein	CDK13_Y716_YF	this paper, synthesized in-house		peptide sequence: Ac-IGEGTYGQVFK-NH2
peptide, recombinant protein	CDK13_Y716_G717R_YF	this paper, synthesized in-house		peptide sequence: Ac-IGEGTYRQVFK-NH2
peptide, recombinant protein	CDK5_Y15	sequence from PMID: 35606422, purchased from Synpeptide		peptide sequence: Ac-IGEGTYGTVFK-NH2
peptide, recombinant protein	CDK5_Y15_G16R	sequence from PMID: 35606422, purchased from Synpeptide		peptide sequence: Ac-IGEGTYRTVFK-NH2
peptide, recombinant protein	PLCG1_Y210	this paper, synthesized in-house		peptide sequence: Ac-SGDITYGQFAQ-NH2
peptide, recombinant protein	PLCG1_Y210_T209N	this paper, synthesized in-house		peptide sequence: Ac-SGDINYGQFAQ-NH2
peptide, recombinant protein	GLB1_Y294	this paper, synthesized in-house		peptide sequence: Ac-VASSLYDILAR-NH2
peptide, recombinant protein	GLB1_Y294_L297F	this paper, synthesized in-house		peptide sequence: Ac-VASSLYDIFAR-NH2
peptide, recombinant protein	ITGA3_Y237_YF	this paper, synthesized in-house		peptide sequence: Ac-WDLSEYSFKDP-NH2
peptide, recombinant protein	ITGA3_Y237_S235P_YF	this paper, synthesized in-house		peptide sequence: Ac-WDLPEYSFKDP-NH2
peptide, recombinant protein	ACTA1_Y171_YF	this paper, synthesized in-house		peptide sequence: Ac-QPIFEG(pY)ALPHAG-NH2
peptide, recombinant protein	ACTA1_Y171_A172G_YF	this paper, synthesized in-house		peptide sequence: Ac-QPIFEG(pY)GLPHAG-NH2
peptide, recombinant protein	ACTB_Y240	this paper, synthesized in-house		peptide sequence: Ac-QSLEKS(pY)ELPDGG-NH2
peptide, recombinant protein	ACTB_Y240_P243L	this paper, synthesized in-house		peptide sequence: Ac-QSLEKS(pY)ELLDGG-NH2
peptide, recombinant protein	CCDC39_Y593	this paper, synthesized in-house		peptide sequence: Ac-QRKQQL(pY)TAMEEG-NH2
peptide, recombinant protein	CLIP2_Y972	this paper, synthesized in-house		peptide sequence: Ac-QSDQRR(pY)SLIDRG-NH2

peptide, recombinant protein	CLIP2_Y972_R977P	this paper, synthesized in-house		peptide sequence: Ac-QSDQRR(pY)SLIDPG-NH2
peptide, recombinant protein	CBS_Y308	this paper, synthesized in-house		peptide sequence: Ac-QVEGIG(pY)DFIPTG-NH2
peptide, recombinant protein	CBS_Y308_G307S	this paper, synthesized in-house		peptide sequence: Ac-QVEGIS(pY)DFIPTG-NH2
peptide, recombinant protein	fluorescently-labeled c-Src-SH2 consensus peptide	sequence from PMID: 7680959		peptide sequence: FITC-Ahx-GDG(pY)EEISPLLL-NH2; gift from Jeanine Amacher at Western Washignton University
commercial assay or kit	MiSeq Reagent Kit v3 (150 cycles)	Illumina	Illumina: MS-102-3001	
commercial assay or kit	NextSeq 500 Mid-Output v2 Kit (150 cycles)	Illumina	Illumina: FC-404-2001	
commercial assay or kit	Promega QuantiFluor™ dsDNA Sample Kit	Promega	Promega: E2671	
commercial assay or kit	ADP Quest Assay Kit	Eurofins Discoverx	Eurofins Discoverx: 90-0071	
commercial assay or kit	Dynabeads™ FlowComp™ Flexi Kit	ThermoFisher Scientific	ThermoFisher Scientific: 11061D	
chemical compound, drug	4-carboxymethyl phenylalanine (CMF)	Millipore Sigma	Millipore Sigma: ENA423210770	
chemical compound, drug	4-azido-L-phenylalanine (AzF)	Chem-Impex International	Chem-Impex: 06162	
chemical compound, drug	N-ε-Acetyl-L-Lysine (AcK)	MP Biomedicals	MP Biomedicals: 02150235.2	
other	Creatine Phosphokinase from rabbit muscle	Millipore Sigma	Millipore Sigma: C3755-500UN	
software, algorithm	FLASH (version FLASH2-2.2.00)	PMID: 21903629		https://ccb.jhu.edu/software/FLASH/
software, algorithm	Cutadapt (version 3.5)	DOI: 10.14806/ej.17.1.200		https://cutadapt.readthedocs.io/en/stable/
software, algorithm	Python scripts for processing and analysis of adeep sequencing data	this paper		https://github.com/nshahlab/2022_Li-et-al_peptide-display

Expression and purification of tyrosine kinase domains

Constructs for the kinase domains of c-Src, c-Abl, Fyn, Hck, AncSZ, Fer, Fes, FGFR1, FGFR3, EPHB1, EPHB2, and MERTK all contained an N-terminal His_6-tag followed by a TEV protease cleavage site. These proteins were co-expressed in *E. coli* BL21(DE3) cells with the YopH tyrosine phosphatase. Cells transformed with YopH and the tyrosine kinase domains were grown in LB supplemented with 100 µg/mL ampicillin and 100 µg/mL streptomycin at 37°C. Once cells reached an optical density of 0.5 at

600 nm, 1 mM of Isopropyl-β-D-1-thiogalactopyranoside (IPTG) was added to induce the expression of proteins and the cultures were incubated at 18°C for 14-16 hours. Cells were harvested by centrifugation (4,000 rpm at 4°C for 30 minutes), resuspended in a lysis buffer containing 50 mM Tris, pH 7.5, 300 mM NaCl, 20 mM imidazole, 2 mM β-mercaptoethanol (BME), 10% glycerol, and lysed using sonication (Fisherbrand Sonic Dismembrator). After separation of insoluble material by centrifugation (33,000 g at 4°C for 45 minutes), the supernatant was applied to a 5 mL HisTrap Ni-NTA column (Cytiva). The resin was washed with 10 column volumes of lysis buffer and wash buffer containing 50 mM Tris, pH 8.5, 50 mM NaCl, 20 mM imidazole, 2 mM BME, 10% glycerol. The protein was eluted with 50 mM Tris, pH 8.5, 50 mM NaCl, 500 mM imidazole, 2 mM BME, and 10% glycerol.

The eluted protein was further purified by anion exchange on a 5 mL HiTrap Q column (Cytiva) and eluted with a gradient of 50 mM to 1 M NaCl in 50 mM Tris, pH 8.5, 1 mM TCEP-HCl and 10% glycerol. The His_6-TEV tag of the collected fractions were cleaved by the addition of 0.10 mg/mL TEV protease overnight. The reaction mixture was subsequently flowed through 2 mL of Ni-NTA resin (ThermoFisher). The cleaved protein was collected in the flow-through and washes, then concentrated by centrifugation in an Amicon™ Ultra-15 30 kDa MWCO spin filter (Millipore). The concentrate was separated on a Superdex 75 16/600 gel filtration column (Cytiva), equilibrated with 10mM HEPES, pH 7.5, 100mM NaCl, 1mM TCEP, 5 mM $MgCl_2$, 10% glycerol. Pure fractions were pooled, aliquoted, and flash frozen in liquid N_2 for long-term storage at -80 °C.

Expression and purification of biotinylated SH2 domains

Grb2 SH2 (56-152), c-Src SH2 (143-250), and SHP2 CSH2 (105-220) domains were cloned into a His_6-SUMO-SH2-Avi construct and were co-expressed with biotin ligase BirA in *E. coli* C43(DE3) cells. Specifically, cells transformed with both BirA and SH2 domains were grown in LB supplemented with 100 µg/mL kanamycin and 100 µg/mL streptomycin at 37 °C until cells reached an optical density of 0.5 at 600 nm. The temperature was brought down to 18 °C, protein expression was induced with 1 mM IPTG, and the media was also supplemented with 250 µM biotin to facilitate biotinylation of the Avi-tagged SH2 domains *in vivo*. Proteins expression was carried out at 18 °C for 14-16 hours. After removal of media by centrifugation, the cells were resuspended in a lysis buffer containing 50 mM Tris, pH 7.5, 300 mM NaCl, 20 mM imidazole, 10% glycerol, and 2 mM BME. The cells were lysed using sonication (Fisherbrand Sonic Dismembrator), and the lysate was clarified by ultracentrifugation. The supernatant was applied to a 5 mL Ni-NTA column (Cytiva). The resin was washed with 10 column volumes each of buffers containing 50 mM Tris, pH 7.5, 300 mM NaCl, 20 mM imidazole, 10% glycerol, and 2 mM BME and 50 mM Tris, pH 7.5, 50 mM NaCl, 20 mM imidazole, 10% glycerol, and 2 mM BME. The protein was eluted in a buffer containing 50 mM Tris pH 7.5, 50 mM NaCl, 500 mM imidazole, 10% Glycerol.

The eluted protein was further purified by ion exchange on a 5 mL HiTrap Q anion exchange column (Cytiva). The following buffers were used: 50 mM Tris, pH 7.5, 50 mM NaCl, 1 mM TCEP and 50 mM Tris, pH 7.5, 1 M NaCl, 1 mM TCEP. The protein was eluted off the column over a salt gradient from 50 mM to 1M NaCl. The His_6-SUMO tag was cleaved by addition of 0.05 mg/mL Ulp1 protease. The reaction mixture was flowed over 2 mL Ni-NTA column (ThermoFisher) to remove the Ulp1, the uncleaved protein, and His_6-SUMO fragments. The cleaved protein was further purified by size-exclusion chromatography on a Superdex 75 16/60 gel filtration column (Cytiva) equilibrated with buffer containing 20 mM HEPES, pH 7.4, 150 mM NaCl, and 10% glycerol. Pure fractions were pooled, aliquoted, and flash frozen in liquid N_2 for long-term storage at -80 °C.

Synthesis and purification of peptides for *in vitro* validation measurements

All the peptides used for *in vitro* kinetic assays were synthesized using 9-fluorenylmethoxycarbonyl (Fmoc) solid-phase peptide chemistry. All syntheses were carried out using the Liberty Blue automated microwave-assisted peptide synthesizer from CEM under nitrogen atmosphere, with standard manufacturer-recommended protocols. Peptides were synthesized on MBHA Rink amide resin solid support (0.1 mmol scale). Each Nα-Fmoc amino acid (6 eq, 0.2 M) was activated

with diisopropylcarbodiimide (DIC, 1.0 M) and ethyl cyano(hydroxyamino)acetate (Oxyma Pure, 1.0 M) in dimethylformamide (DMF) prior to coupling. Each coupling cycle was done at 75 °C for 15 s then 90 °C for 110 s. Deprotection of the Fmoc group was performed in 20% (v/v) piperidine in DMF (75 °C for 15 s then 90 °C for 50 s). The resin was washed (4x) with DMF following Fmoc deprotection and after Nα-Fmoc amino acid coupling. All peptides were acetylated at their N-terminus with 10% (v/v) acetic anhydride in DMF and washed (4x) with DMF.

After peptide synthesis was completed, including N-terminal acetylation, the resin was washed (3x each) with dichloromethane (DCM) and methanol (MeOH) and dried under reduced pressure overnight. The peptides were cleaved and the side chain protecting groups were simultaneously deprotected in 95% (v/v) trifluoroacetic acid (TFA), 2.5% (v/v) triisopropylsilane (TIPS), and 2.5% water (H_2O), in a ratio of 10 µL cleavage cocktail per mg of resin. The cleavage-resin mixture was incubated at room temperature for 90 minutes, with agitation. The cleaved peptides were precipitated in cold diethyl ether, washed in ether, pelleted, and dried under air. The peptides were redissolved in 50% (v/v) water/acetonitrile solution and filtered from the resin.

The crude peptide mixture was purified using reverse-phase high performance liquid chromatography (RP-HPLC) on a semi-preparatory C18 column (Agilent, ZORBAX 300SB-C18, 9.4 x 250 mm, 5 µm) with an Agilent HPLC system (1260 Infinity II). Flow rate was kept at 4 mL/min with solvents A (H_2O, 0.1% (v/v) TFA) and B (acetonitrile, 0.1% (v/v) TFA). Peptides were generally purified over a 40 minute linear gradient from solvent A to solvent B, with the specific gradient depending on the peptide sample. Peptide purity was assessed with an analytical column (Agilent, ZORBAX 300SB-C18, 4.6 x 150 mm, 5 µm) at a flow rate of 1 mL/min over a 0-90% B gradient in 30 minutes. All peptides were determined to be ≥95% pure by peak integration. The identities of the peptides were confirmed by mass spectroscopy (Waters Xevo G2-XS QTOF). Pure peptides were lyophilized and redissolved in 100 mM Tris, pH 8.0, as needed for experiments.

Preparation of the X_5-Y-X_5 and pTyr-Var libraries for specificity profiling

All bacterial display libraries used in this study are embedded within the pBAD33 plasmid (chloramphenicol resistant), with the surface-display construct inducible by L-(+)-arabinose (Rice and Daugherty, 2008). All libraries have the same general structure:

[signal sequence: MKKIACLSALAAVLAFTAGTSVA]-[GQSGQ]-[peptide-coding sequence]-[GGQSGQ]-[eCPX scaffold]-[GGQSGQ]-[strep-tag: WSHPQFEK or myc-tag: EQKLISEEDL]

The X_5-Y-X_5 library contains 11-residue peptide sequences with five randomized amino acids flanking both sides of a fixed central tyrosine residue. The library was produced using the X_5-Y-X_5 library oligo, with each X encoded by an NNS codon, and Y encoded by a TAT codon (see key resources table for all primer sequences). This oligo included a 5' SfiI restriction site and DNA sequences encoding the flanking linkers that connect library peptide sequences to the 5' signal sequence and 3' eCPX scaffold.

The sequences in the pTyr-Var library were derived from the PhosphoSitePlus database and include 3,159 human tyrosine phosphorylation sites and 4,760 variants of these phosphosites bearing a single amino acid mutation (Hornbeck et al., 2019). The sequences in this library are named as "GeneName_pTyr-position" and "GeneName_pTyr-position" (e.g. "SRC_Y530" and "SRC_Y530_527K"). In this initial list, about 2,133 sequences had more than one tyrosine residue, and so a second version of those sequences were included in which the tyrosines except the central tyrosine were substituted with phenylalanine (denoted with a "_YF" suffix). In addition, 24 previously reported consensus substrate sequences were included (Begley et al., 2015; Deng et al., 2014; Marholz et al., 2018; Rube et al., 2022; Songyang et al., 1995). In total, our designed pTyr-Var library contained 9,898 unique 11-residue peptide sequences, which were then converted into DNA sequences using the most frequently used codon in *E. coli*. The DNA sequences were further optimized, swapping synonymous codons to achieve a GC content of all sequence between 30-70%. Sequences were also inspected and altered to remove any internal SfiI recognition sites. The 33-base peptide-coding sequences were flanked by 5'-GCTGGCCAGTCTGGCCAG-3' on the 5' side and 5'- GGAGGGCAGTCTGGGCAGTCTG-3' on the 3'

side, the same flanks used for the X_5-Y-X_5 library oligo. An oligonucleotide pool based on all 9,898 sequences was generated by on-chip massively parallel synthesis (Twist Bioscience). This oligo-pool was amplified by PCR in ten cycles with the Oligopool-fwd-primer and Oligopool-rev-primer, using the NEB Q5 polymerase with a slow ramping speed (2°C/sec) and long denaturation times.

Next, we integrated the oligonucleotide sequences encoding the X_5-Y-X_5 and pTyr-Var library into a pBAD33 vector as a fusion to the eCPX bacterial display scaffold, in a series of steps. The eCPX gene was previously fused to a sequence encoding a 3' strep-tag (pBAD33-eCPX-cStrep) (Shah et al., 2018), and we produced a myc-tagged eCPX construct analogously, using standard molecular cloning techniques (pBAD33-eCPX-cMyc). The coding sequences for the eCPX-strep and eCPX-myc constructs were amplified from these plasmids by PCR using the link-eCPX-fwd primer and the link-eCPX-rev primer. These PCR products contained a 3' SfiI restriction site. The peptide-coding sequences were then fused to the eCPX scaffold at the 5' end of the scaffold in another PCR step to generate the library-scaffold inserts. For the X_5-Y-X_5 Library, this step used the X_5-Y-X_5 library oligo and the link-eCPX-rev primer, along with the amplified eCPX gene. For the pTyr-Var library, this step used the amplified oligo-pool, the amplified eCPX gene, and the Oligopool-fwd-primer and link-eCPX-rev primer. The resulting PCR products contained the peptide-scaffold fusion constructs flanked by two unique SfiI sites.

In parallel, the pBAD33-eCPX backbone was amplified by PCR from the pBAD33-eCPX plasmid using the BB-fwd-primer and BB-rev primer. Both the amplified insert and backbone were purified over spin columns and then digested with the SfiI restriction endonuclease overnight at 50°C. After digestion, the backbone was treated with Quick CIP (NEB) to prevent self-ligation from occurring. Both the digested insert and backbone were gel purified. The purified library insert was ligated into the digested pBAD33-eCPX backbone using T4 DNA ligase (NEB) overnight at 16 °C. Typically, this reaction was done with a total of approximately 1.5 µg of DNA, with a 1:5 molar ratio of backbone:insert. The ligation reaction was concentrated and desalted over a spin column and then used to transform commercial DH5a cells by electroporation. The transformed DH5a cells were grown in liquid culture overnight, and the plasmid DNA was isolated and purified using a commercial midiprep kit (Zymo).

Experimental procedure for high-throughput specificity screening of tyrosine kinases

Preparation of cells displaying peptide libraries

The high-throughput specificity screens for tyrosine kinases using the X_5-Y-X_5 and the pTyr-Var peptide library were carried out as described previously (Shah et al., 2018), with the main difference being the use of magnetic beads to isolate phosphorylated cells, rather than fluorescence-activated cell sorting. 25 µL of electrocompetent *E. coli* MC1061 F- cells were transformed with 200 ng of library DNA. Following electroporation, the cells were resuspended in 1 mL of LB and allowed to recover at 37 °C for 1 hour with shaking. These cells were resuspended in 250 mL of LB with 25 µg/ml chloramphenicol and incubated overnight at 37 °C. 150 µL of the overnight culture was used to inoculate 5.5 mL of LB containing 25 µg/mL chloramphenicol. This culture was grown at 37 °C for 1-2 hours until the cells reached an optical density of 0.5 at 600 nm. Expression of the library was induced by adding arabinose to a final concentration of 0.4% (w/v). The cells were incubated at 25 °C with shaking at 220 rpm for 4 hours. Small aliquots of the cells (75-150 µL) were transferred to microcentrifuge tubes and centrifuged at 1000g at 4 °C for 10-15 minutes. The media was removed and the cells were resuspended in PBS and centrifuged again. The PBS was removed and the cells were stored at 4 °C. Experiments were performed with cells stored at 4 °C between 1-4 days. Typical screens were carried out on a 50 µL to 100 µL scale, with cells that were 50% more concentrated than in culture (OD_{600} value around 1.5). Thus, for a 100 µL reaction, typically 150 µL of cell culture was pelleted and washed.

Phosphorylation of peptides displayed on cells

Phosphorylation reactions of the library were conducted with the purified kinase domain and 1 mM ATP in a buffer containing 50 mM Tris, pH 7.5, 150 mM NaCl, 5 mM $MgCl_2$, 1 mM TCEP, and 2 mM sodium orthovanadate. To achieve similar library phosphorylation levels across the kinases, an optimal concentration of kinase was determined to achieve 20-30% phosphorylation of the library after 3 minutes

of incubation at 37 °C. This was assessed by flow cytometry based on anti-phosphotyrosine antibody labeling (Attune NxT, Invitrogen). To label the phosphorylated cells, 50 µL pellets were resuspended with a 1:25 dilution of the PY20-PerCP-eFluor 710 conjugate (eBioscience) in PBS containing 0.2% bovine serum albumin (BSA). The cells were incubated with the antibody for 1 hr on ice in the dark, then centrifuged, washed once with PBS with 0.2 % BSA, and finally resuspended in 100 µL of PBS with 0.2% BSA. For flow cytometry analysis, 20 µL of cells were diluted in 130 µL of PBS with 0.2% BSA.

The following concentrations were used: 0.5 µM for Src, 1.5 µM for Abl, 0.3 µM for Fes, 0.4 µM for Fer, 1.5 µM for EPHB1, 1.25 µM for EPHB2, 0.1 µM for JAK2, 0.5 µM for AncSZ, 0.45 µM for FGFR1, 0.5 µM for FGFR3, and 0.7 µM for MERTK. For some tyrosine kinases, such as FGFR1, FGFR3, and MERTK, pre-activation with ATP was required to enhance its kinetic activity. To accomplish this, autophosphorylation reactions were performed with 25 µM kinase and 5 mM ATP for 0.5-2 hours at 25 °C. The preactivated kinase mixture was then desalted and concentrated using an Amicon™ Ultra-15 30 kDa MWCO spin filter (Millipore) to remove the residual ATP.

After the desired time of library phosphorylation, kinase activity was quenched with 25 mM EDTA and the cells were washed with PBS containing 0.2% BSA. Kinase-treated cells were then labeled with a 1:1000 dilution of biotinylated 4G10 Platinum anti-phosphotyrosine antibody (Millipore) for an hour on ice and washed with PBS containing 0.1% BSA and 2 mM EDTA (isolation buffer). The cells were finally resuspended in PBS containing 0.1% BSA. The phosphorylated, antibody-labeled cells were then mixed with magnetic beads from Dynabeads® FlowComp™ Flexi kit (Invitrogen), at a ratio of 75 µL of washed beads per 50 µL of cell suspension, diluted into 450 µL of isolation buffer. The suspension was rotated at 4 °C for 30 minutes, then 350 µL of isolation buffer was added and the beads were separated from the bulk solution on a magnetic rack. The beads were washed once with 1 mL of isolation buffer, and then the supertantant were removed by aspiration. The beads were resuspended in 50 µL of fresh water, vortexed, and boiled at 100 °C for 10 minutes to extract DNA from cells bound to Dynabeads. The bead/lysate mixture was centrifuged to pellet the beads and the mixture was stored at -20 °C.

DNA sample preparation and deep sequencing

To amplify the peptide-coding DNA sequence for deep sequencing, the supernatant from this lysate was used as a template in a 50 µL, 15-cycle PCR reaction using the TruSeq-eCPX-Fwd and TruSeq-eCPX-Rev primers and Q5 polymerase. The resulting mixture from this PCR reaction was used without purification as a template for a second, 20 cycle PCR reaction to append a unique pair of Illumina sequencing adapters and 5' and 3' indices for each sample (D700 and D500 series primers). The resulting PCR products were purified by gel extraction, and the concentration of each sample was determined using QuantiFluor® dsDNA System (Promega). Each sample was pooled to equal molarity and sequenced by paired-end Illumina sequencing on a MiSeq or NextSeq instrument using a 150 cycle kit. The number of samples multiplexed in one run, and the loading density on the sequencing chip, were adjusted to obtain at least 1-2 million reads for each index/sample.

<u>Experimental procedure for high-throughput specificity screening of SH2 domains</u>

Phosphorylation of peptides displayed on cells

Bacteria displaying peptide libraries were prepared as described for the kinase screen. Phosphorylation of cells was performed in a buffer containing 50 mM Tris, pH 7.5, 150 mM NaCl, 5 mM $MgCl_2$, 1 mM TCEP. Cells were phosphorylated by addition of a mixture of 2.5 µM of c-Abl kinase domain, 2.5 µM c-Src kinase domain, 2.5 µM of EPHB1 kinase domain, 2.5 µM of AncSZ, 50 µg/mL rabbit muscle creatine phosphokinase, 5 mM creatine phosphate, and 5 mM ATP and incubation at 37 °C for 3 hours. Following this, the kinase activity was quenched by addition of 25 mM EDTA. Library phosphorylation was assessed by flow cytometry based on anti-phosphotyrosine antibody labeling, as described above for the kinase screens (Attune NxT, Invitrogen).

Preparation of magnetic beads functionalized with SH2 domains (SH2-dynabeads)

First, 37.5 µL of magnetic beads from the Dynabeads® FlowComp™ Flexi kit (Invitrogen) were

washed with 1 mL of SH2 screen buffer containing 50 mM HEPES, pH 7.5, 150 mM NaCl. After washing, the beads were resuspended in 75 µL of 20 µM biotinylated SH2 domain and incubated at 4 °C for 2.5-3 hours. Unbound SH2 domain protein was removed by washing twice with 1 mL of SH2 screen buffer twice. The beads were finally resuspended in 37.5 µL of SH2 screen buffer.

Selection with SH2-dynabeads

50 µL of the phosphorylated cells were centrifuged at 4000 g at 4 °C for 15 minutes. After the supernatant was discarded, the cells were resuspended in SH2 screen buffer with 0.1% BSA, mixed with 37.5 µL of SH2-dynabeads, and rotated for 1 hour at 4 °C. Then, the magnetic beads were separated from the bulk solution using a magnetic rack, and the supernatant was removed by aspiration. After the supernatant was discarded, the SH2-beads were washed by incubating them with 1 mL of SH2 screen buffer for 30 minutes at 4 °C. After discarding the wash solution, the beads were resuspended in 50 µL of fresh water, vortexed, and boiled at 100°C for 10 minutes to extract DNA from cells bound to SH2-dynabeads. DNA samples were prepped and sequenced identically as done for the kinase screens.

Procedure for incorporating non-canonical amino acids in the high-throughput specificity screen

General protocol

E.coli MC1061 electrocompetent bacteria were transformed with genetically-encoded peptide libraries and grown in liquid LB media as described in the regular screens, but with an additional plasmid encoding the corresponding non-canonical amino acid aminoacyl synthetase and tRNA pair and the addition of 100 µg/mL ampicillin to the growth medium. The cells were grown to an optical density of 0.5 at 600 nm. Peptide expression was induced with 0.4% (w/v) arabinose, 1 mM isopropyl β-D-1-thiogalactopyranoside (IPTG), and 5 mM CMF, 5 mM AzF, or 10 mM AcK, and incubated at 25 °C for 4 hours. Cell pellets were collected and washed in PBS as described in the regular screens. Bacteria bearing surface-displayed peptides containing the non-canonical amino acid of interest were phosphorylated with 0.5 µM Src kinase for 3 minutes using the same buffer conditions as in the regular kinase screens. The reaction was carried out in buffer containing 50 mM Tris, 150 mM NaCl, 5 mM $MgCl_2$, pH 7.5, 1 mM TCEP, and 2 mM activated sodium orthovanadate for 3 minutes. The reactions were initiated with 1 mM ATP and quenched with 25 mM EDTA, then washed with PBS containing 0.2% BSA, as described for the regular screens. Downstream processing of the samples, including phospho-tyrosine labeling, separation using magnetic beads, and deep sequencing were done exactly as in the regular kinase screens.

Fluorophore labeling of surface-displayed AzF using click chemistry

The DIBO labeling solution was prepared by dissolving 0.5 mg of DIBO-alkyne Alexa Fluor 555 dye (ThermoFisher) in dimethyl sulfoxide (DMSO) to a concentration of 1 mM, and the solution was kept protected from light. The c-Myc tag labeling solution was prepared by a 1:100 dilution of c-Myc Alexa Fluor 488 conjugate (ThermoFisher) in PBS containing 0.2% BSA. The cell pellets treated with AzF were resuspended in 50 µM of the DIBO labeling solution and incubated overnight at RT with gentle nutation, protected from light (Tian et al., 2014). The cell suspension was pelleted and washed 4x in PBS containing 0.2% BSA to ensure all excess DIBO dye was removed. The cell pellets were then resuspended in the c-Myc antibody solution and incubated on ice for 1 hour, protected from light. The cell suspension was pelleted and washed using PBS with 0.2% BSA. The pellets were resuspended in PBS with 0.2% BSA and analyzed by flow cytometry (Attune NxT, Invitrogen).

Processing and analysis of deep sequencing data from high-throughput specificity screens

The raw paired-end reads for each index pair from an Illumina sequencing run were merged using the FLASH (Magoč and Salzberg, 2011). The resulting merged sequences were then searched for the following 5' and 3' flanking sequences surrounding the peptide-coding region of the libraries: 5' flanking sequence = 5'-NNNNNNACCGCAGGTACTTCCGTAGCTGGCCAGTCTGGCCAG-3', and 3' flanking

sequence = 5'-GGAGGGCAGTCTGGGCAGTCTGGTGACTACAACAAAANNNNNN-3'. These flanks were removed using the software Cutadapt to yield a filed named "SampleName.trimmed.fastq" (Martin, 2011). Sequences that did not contain both of these flanking regions were discarded at this stage (typically less than 5%). From this point onward, all analysis was carried out using Python scripts generated in-house, which can be found in a GitHub repository (https://github.com/nshahlab/2022_Li-et-al_peptide-display).

Analysis of data from screens with the pTyr-Var Library

For the samples screened with the pTyr-Var Library, we ran scripts that identify every 33 base trimmed DNA sequence, translate those DNA sequences into amino acid sequences, count the abundance of each translated sequence that matches a peptide in the pTyr-Var library. In one format of this analysis, we used the countPeptides.py script on a trimmed input file, or batch-countPeptides.py script for multiple input files, to generate a list of every unique peptide and its corresponding counts. In a second format of this analysis, we used the countPeptides-var-ref.py (or batch-countPeptides-var-ref.py), along with paired text files listing each variant (pTyr-Var_variant.txt) and their corresponding reference sequence (pTyr-Var_reference.txt), line-by-line, to yield side-by-side counts for each variant-reference pair. These processing steps were conducted for both selected samples (after kinase phosphorylation or SH2 binding), as well as unselected input samples. Next, the number of reads for every sequence ($n_{peptide}$) was normalized to the total number of peptide-coding reads in that sample (n_{total}), to yield a frequency ($f_{peptide}$, equation 1). Then, the frequency of each peptide in a selected sample ($f_{peptide,selected}$) was further normalized to the frequency of that same peptide in the unselected input sample ($f_{peptide,input}$) to yield an enrichment score ($E_{peptide}$, equation 2).

$$(1) \qquad f_{peptide} = \frac{n_{peptide}}{n_{total}} \qquad\qquad (2) \qquad E_{peptide} = \frac{f_{peptide,selected}}{f_{peptide,input}}$$

Analysis of data from screens with the X_5-Y-X_5 Library

For data from the X_5-Y-X_5 library, we did not calculate enrichments for individual sequences, as the sequencing depth per sample was generally on-par with the library size was (10^6-10^7 sequences). Instead, we computed the counts for each amino acid (or a stop codon) at every position along peptides of the expected length (11 amino acid residues). To accomplish this, we first translated all of the DNA sequences in the trimmed sequencing files using the translateUnique.py (or batch-translateUnique.py) script. When stop codons were encountered, they were translated as an asterisk symbol. In addition to producing a file of translated reads named "SampleName.translate.fasta", this script also produced lists of every unique translated 11-residue peptide and the corresponding counts for that peptide. These files allowed us to assess whether any individual sequence was disproportionately enriched (not expected for a single round of selection with a library of this size), how many unique sequences were in each sample, and what fraction of the unique sequences contained a stop codon.

Using the translated read files, we then calculated the position-specific amino acid counts in three formats. In the simplest format, we exclusively counted 11-residue sequences that contained a central tyrosine and no stop codons (AA-count-nostop.py and batch-AA-count-nostop.py). In order to calculate stop codon depletion, we run a version of the script that counted amino acid and stop codon composition across all 11-residue sequences (AA-count-full.py and batch-AA-count-full.py). Finally, for Amber suppression datasets, we exclusively counted sequences containing one stop and a central tyrosine residue (AA-count-1stop.py and batch-AA-count-1stop,py). Each of these scripts generated an 11x21 counts matrix with each position in the peptide represented by a column (from -5 to +5), and each row represented by an amino acid (in alphabetical order, with the stop codon in the 21st row). Frequencies of each amino acid at each position were determined by taking the position-specific count for each amino acid and dividing that by the column total. Frequencies in a matrix from a selected sample were further normalized against frequencies from an input sample, and the resulting enrichment values were log_2-transformed to yield the data represented in the heatmaps in Figures 1, 2, 6, and 7.

Scoring sequences using data from the X_5-Y-X_5 Library

In order to score peptides using position-weighted counts matrixes from the X_5-Y-X_5 Library, we

wrote a Python script called score_peptide_nostop.py. This script requires the selected and input counts matrices for a kinase or SH2 domain, produced by the AA-count-nostop.py script, along with a list of peptides as a text file, with one peptide per line. The script first calculates the normalized enrichments for each amino acid at each position across the matrices. Then, it reads each target sequence, sums up the $\log_2$-normalized enrichments for each residue according to the enrichment matrix, ignoring the central tyrosine, and divides the sum by the number of scored residues (10 for the X_5-Y-X_5 Library). The script also calculates the score for the best and worst sequence, according to the enrichment matrix. Both unnormalized and normalized scores for the whole peptide list are outputted as text files.

In vitro measurements of phosphorylation rates with purified kinases and peptides

RP-HPLC assay to measure peptide phosphorylation kinetics

To validate the enrichment scores observed in the c-Src screening data, the phosphorylation rates were measured *in vitro* with the purified catalytic domain of c-Src and synthetic 11-residue peptides derived from sequences in the pTyr-Var library. Kinetic measurements were carried out at 37 °C by mixing 500 nM c-Src and 100 μM peptide in a buffer containing 50 mM Tris, pH 7.5, 150 mM NaCl, 5 mM $MgCl_2$, 1 mM TCEP, and 2 mM activated sodium orthovanadate. Reactions were initiated by adding 1 mM ATP. At various time points, 100 μL aliquots were removed and quenched by the addition of EDTA to a final concentration of 25 mM. Each time point sample was analyzed by analytical RP-HPLC, monitoring absorbance at 214 nm. 40 μL of each time point was injected onto a C18 column (ZORBAX 300SB-C18, 5 μm, 4.6 x 150 mm). The solvent system used was water with 0.1% trifluoroacetic acid (solvent A) and acetonitrile with 0.1% trifluoroacetic acid (solvent B). Peptides were eluted at a flow rate of 1 mL/min, using the following set of linear gradients: 0-2 minutes: 5% B, 2-12 minutes: 5-95% B, 12-13 minutes: 95% B, 13-14 minutes: 95-5% B, and 14-17 minutes: 5% B. The areas under the peaks corresponding to the unphosphorylated and phosphorylated peptides were calculated using the Agilent OpenLAB ChemStation software. The fractional product peak area was plotted as a function of reaction time, and the initial linear regime of this plot was fitted to a straight line to determine a reaction rate. Rates were corrected for substrate and enzyme concentration. Reactions were done in triplicate or quadruplicate.

Michaelis-Menten analysis using the ADP-Quest assay

A fluorescence-based assay from Eurofins (ADP Quest) was used to measure the Michaelis-Menten kinetic parameters for phosphorylation of the consensus peptides by purified tyrosine kinase domains. In this assay, ADP production as a result of kinase activity is coupled to the production of resorufin, a fluorophore that emits signal at 590 nm. For all experiments, the assay reactions were set up as described in the provided assay kit protocol, in a 384 well plate format**.** The peptide solutions were serially diluted in 100 mM Tris, pH 8.0, and the kinases were diluted to 50 nM in buffer (10 mM HEPES, 100 mM NaCl, 1 mM TCEP, 5 mM $MgCl_2$, 10% (v/v) glycerol). The final reaction mixtures contained 10 nM of kinase with 100 μM of ATP. Reactions were initiated with the addition of 1 mM ATP into a 50 μL reaction mixture for a final concentration of 100 μM ATP. Phosphorylation reaction progress was monitored by measuring fluorescence at excitation 530 nm and emission 590 nm every 2 minutes at 37 °C on a plate reader (BioTek Synergy Neo 2). The fluorescence units (RFU) were converted to μM ADP by comparison to a standard curve, and the initial rates were extracted from the linear regime of the reaction progress curves. Initial rates were also measured for samples containing each kinase but lacking a peptide substrate, to account for background ATP hydrolysis. This background rate was subtracted from the rates measured in the presence of peptide. The subtracted rates were plotted as a function of substrate concentration and fit to the Michaelis-Menten equation to extract k_{cat} and K_M values.

In vitro measurements of binding affinities with purified SH2 and phospho-peptides

Binding affinities of SH2 domains and phospho-peptides were measured using fluorescence polarization-based competition binding assay, following previously reported methods (Cushing et al., 2008). The fluorescent peptide (FITC-Acp-GDG(pY)EEISPLLL) used for K_D measurements was a gift

from the Amacher lab. A buffer containing 60 mM HEPES, pH 7.2, 75 mM KCl, 75 mM NaCl, 1 mM EDTA, and 0.05% Tween 20 was used for the experiments. For K_D measurement, varying concentrations of the c-Src SH2 protein were incubated with 30 nM fluorescent peptide for 15 minutes in a black, half-area, 96-well plate. The plate was centrifuged for 5 minutes at 1000 g to remove air bubbles. Following this, fluorescence polarization data was collected on a plate reader at 25 °C (BioTek Synergy Neo 2). The samples were excited at a wavelength of 485 nm and emission data was collected at 525 nm. Data was analyzed and fitted to a quadratic binding equation to determine the K_D for the fluorescent peptide with c-Src. A K_D of 160 nM was obtained for the fluorescent peptide with the c-Src SH2 domain, and this value was used in subsequent calculations for the competition binding experiments.

Competition binding experiments were performed similarly. A stock solution was prepared by mixing 60 nM fluorescent peptide with SH2 domain at a concentration of 480 nM (3x K_D) and incubated at room temp for 15 minutes. Unlabeled competitor peptide was serially diluted in buffer. Each serial dilution was mixed with fluorescent peptide-SH2 stock solution at a 1:1 ratio in a black, half-area, 96 well plate. After mixing the samples by pipetting, the plate was centrifuged at 1000 g for 5 minutes to remove air bubbles. The final fluorescent peptide concentration was 30 nM and the final SH2 concentration was 1.5x K_D (240 nM). Fluoresce polarization was measured as previously described for initial K_D measurements. Competition binding data were fit to a cubic binding equation as described previously (Cushing et al., 2008).

Acknowledgements

We thank Fereshteh Zandkarimi and Brandon Fowler from the Columbia Chemistry mass spectrometry facility for their assistance with mass spectrometry; Jia Ma from the Columbia Precision Biomolecular Characterization Facility for his guidance with biophysical measurements; and the Columbia Genome Center for their support with deep sequencing. We thank Harmen Bussemaker, Tomas Rube, and Chaitanya Rastogi for their insightful discussions, and members of the Shah lab for their technical and conceptual guidance throughout this project. The fluorescently-labeled c-Src SH2 ligand was a gift from the Jeanine Amacher. The pULTRA chAcKRS3 plasmid was a gift from Abhishek Chatterjee. Bacterial expression vectors for Fer, Fes, FGFR1, FGFR3, EPHB1, EPHB2, and MERTK were gifts from John Chodera, Nicholas Levinson, and Markus Seeliger (Addgene plasmid #s 79686, 79719, 79731, 79694, 79697, and 79705). The pEVOL pAzFRS.2.t1 plasmid was a gift from Farren Isaacs (Addgene plasmid #73546). This work was supported by NIH grant R35 GM138014 and a Damon Runyon-Dale F. Frey Award for Breakthrough Scientists (DFS 31-18), awarded to NHS.

Competing interests

The authors declare no competing interests.

References

Albanese SK, Parton DL, Işık M, Rodríguez-Laureano L, Hanson SM, Behr JM, Gradia S, Jeans C, Levinson NM, Seeliger MA, Chodera JD. 2018. An open library of human kinase domain constructs for automated bacterial expression. *Biochemistry* **57**:4675–4689. doi:10.1021/acs.biochem.7b01081

Alexander J, Lim D, Joughin BA, Hegemann B, Hutchins JRA, Ehrenberger T, Ivins F, Sessa F, Hudecz O, Nigg EA, Fry AM, Musacchio A, Stukenberg PT, Mechtler K, Peters J-M, Smerdon SJ, Yaffe MB. 2011. Spatial exclusivity combined with positive and negative selection of phosphorylation motifs is the basis for context-dependent mitotic signaling. *Sci Signal* **4**:ra42. doi:10.1126/scisignal.2001796

Alfaro-Lopez J, Yuan W, Phan BC, Kamath J, Lou Q, Lam KS, Hruby VJ. 1998. Discovery of a novel series of potent and selective substrate-based inhibitors of p60c-src protein tyrosine kinase: conformational and topographical constraints in peptide design. *J Med Chem* **41**:2252–2260. doi:10.1021/jm9707885

Amanchy R, Zhong J, Molina H, Chaerkady R, Iwahori A, Kalume DE, Grønborg M, Joore J, Cope L, Pandey A. 2008. Identification of c-Src tyrosine kinase substrates using mass spectrometry and peptide microarrays. *J Proteome Res* **7**:3900–3910. doi:10.1021/pr800198w

Amiram M, Haimovich AD, Fan C, Wang Y-S, Aerni H-R, Ntai I, Moonan DW, Ma NJ, Rovner AJ, Hong SH, Kelleher NL, Goodman AL, Jewett MC, Söll D, Rinehart J, Isaacs FJ. 2015. Evolution of translation machinery in recoded bacteria enables multi-site incorporation of nonstandard amino acids. *Nat Biotechnol* **33**:1272–1279. doi:10.1038/nbt.3372

Barber KW, Miller CJ, Jun JW, Lou HJ, Turk BE, Rinehart J. 2018a. Kinase Substrate Profiling Using a Proteome-wide Serine-Oriented Human Peptide Library. *Biochemistry* **57**:4717–4725. doi:10.1021/acs.biochem.8b00410

Barber KW, Muir P, Szeligowski RV, Rogulina S, Gerstein M, Sampson JR, Isaacs FJ, Rinehart J. 2018b. Encoding human serine phosphopeptides in bacteria for proteome-wide identification of phosphorylation-dependent interactions. *Nat Biotechnol* **36**:638–644. doi:10.1038/nbt.4150

Begley MJ, Yun C, Gewinner CA, Asara JM, Johnson JL, Coyle AJ, Eck MJ, Apostolou I, Cantley LC. 2015. EGF-receptor specificity for phosphotyrosine-primed substrates provides signal integration with Src. *Nat Struct Mol Biol* **22**:983–990. doi:10.1038/nsmb.3117

Bose R, Holbert MA, Pickin KA, Cole PA. 2006. Protein tyrosine kinase-substrate interactions. *Curr Opin Struct Biol* **16**:668–675. doi:10.1016/j.sbi.2006.10.012

Bradley D, Viéitez C, Rajeeve V, Selkrig J, Cutillas PR, Beltrao P. 2021. Sequence and Structure-Based Analysis of Specificity Determinants in Eukaryotic Protein Kinases. *Cell Rep* **34**:108602. doi:10.1016/j.celrep.2020.108602

Cantor AJ, Shah NH, Kuriyan J. 2018. Deep mutational analysis reveals functional trade-offs in the sequences of EGFR autophosphorylation sites. *Proc Natl Acad Sci USA* **115**:E7303–E7312. doi:10.1073/pnas.1803598115

Chapelat J, Berst F, Marzinzik AL, Moebitz H, Drueckes P, Trappe J, Fabbro D, Seebach D. 2012. The Substrate-Activity-Screening methodology applied to receptor tyrosine kinases: a proof-of-concept study. *Eur J Med Chem* **57**:1–9. doi:10.1016/j.ejmech.2012.08.038

Chatterjee A, Sun SB, Furman JL, Xiao H, Schultz PG. 2013. A versatile platform for single- and multiple-unnatural amino acid mutagenesis in Escherichia coli. *Biochemistry* **52**:1828–1837. doi:10.1021/bi4000244

Chou MF, Prisic S, Lubner JM, Church GM, Husson RN, Schwartz D. 2012. Using bacteria to determine protein kinase specificity and predict target substrates. *PLoS ONE* **7**:e52747. doi:10.1371/journal.pone.0052747

Corwin T, Woodsmith J, Apelt F, Fontaine J-F, Meierhofer D, Helmuth J, Grossmann A, Andrade-Navarro MA, Ballif BA, Stelzl U. 2017. Defining human tyrosine kinase phosphorylation networks using yeast as an in vivo model substrate. *Cell Syst* **5**:128-139.e4. doi:10.1016/j.cels.2017.08.001

Creixell P, Palmeri A, Miller CJ, Lou HJ, Santini CC, Nielsen M, Turk BE, Linding R. 2015a. Unmasking determinants of specificity in the human kinome. *Cell* **163**:187–201. doi:10.1016/j.cell.2015.08.057

Creixell P, Schoof EM, Simpson CD, Longden J, Miller CJ, Lou HJ, Perryman L, Cox TR, Zivanovic N, Palmeri A, Wesolowska-Andersen A, Helmer-Citterich M, Ferkinghoff-Borg J, Itamochi H, Bodenmiller B, Erler JT, Turk BE, Linding R. 2015b. Kinome-wide decoding of network-attacking mutations rewiring cancer signaling. *Cell* **163**:202–217. doi:10.1016/j.cell.2015.08.056

Cujec TP, Medeiros PF, Hammond P, Rise C, Kreider BL. 2002. Selection of v-abl tyrosine kinase substrate sequences from randomized peptide and cellular proteomic libraries using mRNA display. *Chem Biol* **9**:253–264. doi:10.1016/s1074-5521(02)00098-4

Cunningham JM, Koytiger G, Sorger PK, AlQuraishi M. 2020. Biophysical prediction of protein-peptide interactions and signaling networks using machine learning. *Nat Methods* **17**:175–183. doi:10.1038/s41592-019-0687-1

Cushing PR, Fellows A, Villone D, Boisguérin P, Madden DR. 2008. The relative binding affinities of PDZ partners for CFTR: a biochemical basis for efficient endocytic recycling. *Biochemistry* **47**:10084–10098. doi:10.1021/bi8003928

Deng Y, Alicea-Velázquez NL, Bannwarth L, Lehtonen SI, Boggon TJ, Cheng H-C, Hytönen VP, Turk BE. 2014. Global analysis of human nonreceptor tyrosine kinase specificity using high-density peptide microarrays. *J Proteome Res* **13**:4339–4346. doi:10.1021/pr500503q

Dente L, Vetriani C, Zucconi A, Pelicci G, Lanfrancone L, Pelicci PG, Cesareni G. 1997. Modified phage peptide libraries as a tool to study specificity of phosphorylation and recognition of tyrosine containing peptides. *J Mol Biol* **269**:694–703. doi:10.1006/jmbi.1997.1073

Encinas M, Crowder RJ, Milbrandt J, Johnson EM. 2004. Tyrosine 981, a novel ret autophosphorylation site, binds c-Src to mediate neuronal survival. *J Biol Chem* **279**:18262–18269. doi:10.1074/jbc.M400505200

Filippakopoulos P, Kofler M, Hantschel O, Gish GD, Grebien F, Salah E, Neudecker P, Kay LE, Turk BE, Superti-Furga G, Pawson T, Knapp S. 2008. Structural coupling of SH2-kinase domains links Fes and Abl substrate recognition and kinase activation. *Cell* **134**:793–803. doi:10.1016/j.cell.2008.07.047

Finneran P, Soucheray M, Wilson C, Otten R, Buosi V, Krogan NJ, Swaney DL, Theobald DL, Kern D. 2020. Bimodal evolution of Src and Abl kinase substrate specificity revealed using mammalian cell extract as substrate pool. *BioRxiv*. doi:10.1101/2020.08.12.248104

Gram H, Schmitz R, Zuber JF, Baumann G. 1997. Identification of phosphopeptide ligands for the Src-homology 2 (SH2) domain of Grb2 by phage display. *Eur J Biochem* **246**:633–637. doi:10.1111/j.1432-1033.1997.00633.x

Gräslund S, Savitsky P, Müller-Knapp S. 2017. In Vivo Biotinylation of Antigens in E. coli. *Methods Mol Biol* **1586**:337–344. doi:10.1007/978-1-4939-6887-9_22

Henriques ST, Thorstholm L, Huang Y-H, Getz JA, Daugherty PS, Craik DJ. 2013. A novel quantitative kinase assay using bacterial surface display and flow cytometry. *PLoS ONE* **8**:e80474. doi:10.1371/journal.pone.0080474

Hobbs HT, Shah NH, Shoemaker SR, Amacher JF, Marqusee S, Kuriyan J. 2022. Saturation mutagenesis of a predicted ancestral Syk-family kinase. *BioRxiv*. doi:10.1101/2022.04.24.489292

Hornbeck PV, Kornhauser JM, Latham V, Murray B, Nandhikonda V, Nord A, Skrzypek E, Wheeler T, Zhang B, Gnad F. 2019. 15 years of PhosphoSitePlus®: integrating post-translationally modified sites, disease variants and isoforms. *Nucleic Acids Res* **47**:D433–D441. doi:10.1093/nar/gky1159

Hornbeck PV, Zhang B, Murray B, Kornhauser JM, Latham V, Skrzypek E. 2015. PhosphoSitePlus, 2014: mutations, PTMs and recalibrations. *Nucleic Acids Res* **43**:D512-20. doi:10.1093/nar/gku1267

Huang H, Li L, Wu C, Schibli D, Colwill K, Ma S, Li C, Roy P, Ho K, Songyang Z, Pawson T, Gao Y, Li SS-C. 2008. Defining the specificity space of the human SRC homology 2 domain. *Mol Cell Proteomics* **7**:768–784. doi:10.1074/mcp.M700312-MCP200

Hutti JE, Jarrell ET, Chang JD, Abbott DW, Storz P, Toker A, Cantley LC, Turk BE. 2004. A rapid method for determining protein kinase phosphorylation specificity. *Nat Methods* **1**:27–29. doi:10.1038/nmeth708

Imhof D, Wavreille A-S, May A, Zacharias M, Tridandapani S, Pei D. 2006. Sequence specificity of SHP-1 and SHP-2 Src homology 2 domains. Critical roles of residues beyond the pY+3 position. *J Biol Chem* **281**:20271–20282. doi:10.1074/jbc.M601047200

Johnson JL, Yaron TM, Huntsman EM, Kerelsky A, Song J, Regev A, Lin T-Y, Liberatore K, Cizin DM, Cohen BM, Vasan N, Ma Y, Krismer K, Torres Robles J, van de Kooij B, van Vlimmeren AE, Andrée-Busch N, Käufer NF, Dorovkov MV, Ryazanov AG, Cantley LC. 2022. A global atlas of substrate specificities for the human serine/threonine kinome. *BioRxiv*. doi:10.1101/2022.05.22.492882

Jones RB, Gordus A, Krall JA, MacBeath G. 2006. A quantitative protein interaction network for the ErbB receptors using protein microarrays. *Nature* **439**:168–174. doi:10.1038/nature04177

Kaneko T, Huang H, Zhao B, Li L, Liu H, Voss CK, Wu C, Schiller MR, Li SS-C. 2010. Loops govern SH2 domain specificity by controlling access to binding pockets. *Sci Signal* **3**:ra34. doi:10.1126/scisignal.2000796

Kang X, Kim J, Deng M, John S, Chen H, Wu G, Phan H, Zhang CC. 2016. Inhibitory leukocyte immunoglobulin-like receptors: Immune checkpoint proteins and tumor sustaining factors. *Cell Cycle* **15**:25–40. doi:10.1080/15384101.2015.1121324

Kessels HWHG, Ward AC, Schumacher TNM. 2002. Specificity and affinity motifs for Grb2 SH2-ligand interactions. *Proc Natl Acad Sci USA* **99**:8524–8529. doi:10.1073/pnas.142224499

Koytiger G, Kaushansky A, Gordus A, Rush J, Sorger PK, MacBeath G. 2013. Phosphotyrosine signaling proteins that drive oncogenesis tend to be highly interconnected. *Mol Cell Proteomics* **12**:1204–1213. doi:10.1074/mcp.M112.025858

Krassowski M, Paczkowska M, Cullion K, Huang T, Dzneladze I, Ouellette BFF, Yamada JT, Fradet-Turcotte A, Reimand J. 2018. ActiveDriverDB: human disease mutations and genome variation in post-translational modification sites of proteins. *Nucleic Acids Res* **46**:D901–D910. doi:10.1093/nar/gkx973

Kundu K, Costa F, Huber M, Reth M, Backofen R. 2013. Semi-supervised prediction of SH2-peptide interactions from imbalanced high-throughput data. *PLoS ONE* **8**:e62732. doi:10.1371/journal.pone.0062732

Lam KS, Sroka T, Chen ML, Zhao Y, Lou Q, Wu J, Zhao ZG. 1998. Application of “one-bead one-compound” combinatorial library methods in signal transduction research. *Life Sci* **62**:1577–1583. doi:10.1016/s0024-3205(98)00110-6

Landrum MJ, Lee JM, Benson M, Brown GR, Chao C, Chitipiralla S, Gu B, Hart J, Hoffman D, Jang W, Karapetyan K, Katz K, Liu C, Maddipatla Z, Malheiro A, McDaniel K, Ovetsky M, Riley G, Zhou G, Holmes JB, Maglott DR. 2018. ClinVar: improving access to variant interpretations and supporting evidence. *Nucleic Acids Res* **46**:D1062–D1067. doi:10.1093/nar/gkx1153

Lim WA, Pawson T. 2010. Phosphotyrosine signaling: evolving a new cellular communication system. *Cell* **142**:661–667. doi:10.1016/j.cell.2010.08.023

Lin W, Mehta S, Zhang J. 2019. Genetically encoded fluorescent biosensors illuminate kinase signaling in cancer. *J Biol Chem* **294**:14814–14822. doi:10.1074/jbc.REV119.006177

Liu H, Huang H, Voss C, Kaneko T, Qin WT, Sidhu S, Li SS-C. 2019. Surface loops in a single SH2 domain are capable of encoding the spectrum of specificity of the SH2 family. *Mol Cell Proteomics* **18**:372–382. doi:10.1074/mcp.RA118.001123

Liu X, Brodeur SR, Gish G, Songyang Z, Cantley LC, Laudano AP, Pawson T. 1993. Regulation of c-Src tyrosine kinase activity by the Src SH2 domain. *Oncogene* **8**:1119–1126.

Lo W-L, Shah NH, Rubin SA, Zhang W, Horkova V, Fallahee IR, Stepanek O, Zon LI, Kuriyan J, Weiss A. 2019. Slow phosphorylation of a tyrosine residue in LAT optimizes T cell ligand discrimination. *Nat Immunol* **20**:1481–1493. doi:10.1038/s41590-019-0502-2

Lubner JM, Balsbaugh JL, Church GM, Chou MF, Schwartz D. 2018. Characterizing protein kinase substrate specificity using the proteomic peptide library (propel) approach. *Curr Protoc Chem Biol* **10**:e38. doi:10.1002/cpch.38

Lundby A, Franciosa G, Emdal KB, Refsgaard JC, Gnosa SP, Bekker-Jensen DB, Secher A, Maurya SR, Paul I, Mendez BL, Kelstrup CD, Francavilla C, Kveiborg M, Montoya G, Jensen LJ, Olsen JV. 2019. Oncogenic mutations rewire signaling pathways by switching protein recruitment to phosphotyrosine sites. *Cell* **179**:543-560.e26. doi:10.1016/j.cell.2019.09.008

Lu Y, Yu Q, Liu JH, Zhang J, Wang H, Koul D, McMurray JS, Fang X, Yung WKA, Siminovitch KA, Mills GB. 2003. Src family protein-tyrosine kinases alter the function of PTEN to regulate phosphatidylinositol 3-kinase/AKT cascades. *J Biol Chem* **278**:40057–40066. doi:10.1074/jbc.M303621200

Magoč T, Salzberg SL. 2011. FLASH: fast length adjustment of short reads to improve genome assemblies. *Bioinformatics* **27**:2957–2963. doi:10.1093/bioinformatics/btr507

Marholz LJ, Zeringo NA, Lou HJ, Turk BE, Parker LL. 2018. In silico design and in vitro characterization of universal tyrosine kinase peptide substrates. *Biochemistry* **57**:1847–1851. doi:10.1021/acs.biochem.8b00044

Martin M. 2011. Cutadapt removes adapter sequences from high-throughput sequencing reads. *EMBnet j* **17**:10. doi:10.14806/ej.17.1.200

Miller ML, Jensen LJ, Diella F, Jørgensen C, Tinti M, Li L, Hsiung M, Parker SA, Bordeaux J, Sicheritz-Ponten T, Olhovsky M, Pasculescu A, Alexander J, Knapp S, Blom N, Bork P, Li S, Cesareni G, Pawson T, Turk BE, Linding R. 2008. Linear motif atlas for phosphorylation-dependent signaling. *Sci Signal* **1**:ra2. doi:10.1126/scisignal.1159433

Mok J, Im H, Snyder M. 2009. Global identification of protein kinase substrates by protein microarray analysis. *Nat Protoc* **4**:1820–1827. doi:10.1038/nprot.2009.194

Mok J, Kim PM, Lam HYK, Piccirillo S, Zhou X, Jeschke GR, Sheridan DL, Parker SA, Desai V, Jwa M, Cameroni E, Niu H, Good M, Remenyi A, Ma J-LN, Sheu Y-J, Sassi HE, Sopko R, Chan CSM, De Virgilio C, Turk BE. 2010. Deciphering protein kinase specificity through large-scale analysis of yeast phosphorylation site motifs. *Sci Signal* **3**:ra12. doi:10.1126/scisignal.2000482

Morimatsu M, Takagi H, Ota KG, Iwamoto R, Yanagida T, Sako Y. 2007. Multiple-state reactions between the epidermal growth factor receptor and Grb2 as observed by using single-molecule analysis. *Proc Natl Acad Sci USA* **104**:18013–18018. doi:10.1073/pnas.0701330104

Ning X, Guo J, Wolfert MA, Boons G-J. 2008. Visualizing Metabolically Labeled Glycoconjugates of Living Cells by Copper-Free and Fast Huisgen Cycloadditions. *Angew Chem Int Ed* **120**:2285–2287. doi:10.1002/ange.200705456

Obenauer JC, Cantley LC, Yaffe MB. 2003. Scansite 2.0: Proteome-wide prediction of cell signaling interactions using short sequence motifs. *Nucleic Acids Res* **31**:3635–3641. doi:10.1093/nar/gkg584

Oh D, Ogiue-Ikeda M, Jadwin JA, Machida K, Mayer BJ, Yu J. 2012. Fast rebinding increases dwell time of Src homology 2 (SH2)-containing proteins near the plasma membrane. *Proc Natl Acad Sci USA* **109**:14024–14029. doi:10.1073/pnas.1203397109

Parker BL, Shepherd NE, Trefely S, Hoffman NJ, White MY, Engholm-Keller K, Hambly BD, Larsen MR, James DE, Cordwell SJ. 2014. Structural basis for phosphorylation and lysine acetylation cross-talk in a kinase motif associated with myocardial ischemia and cardioprotection. *J Biol Chem* **289**:25890–25906. doi:10.1074/jbc.M114.556035

Pawson T, Nash P. 2000. Protein-protein interactions define specificity in signal transduction. *Genes Dev* **14**:1027–1047.

Rahuel J, Gay B, Erdmann D, Strauss A, Garcia-Echeverría C, Furet P, Caravatti G, Fretz H, Schoepfer J, Grütter MG. 1996. Structural basis for specificity of Grb2-SH2 revealed by a novel ligand binding mode. *Nat Struct Biol* **3**:586–589. doi:10.1038/nsb0796-586

Ren L, Chen X, Luechapanichkul R, Selner NG, Meyer TM, Wavreille A-S, Chan R, Iorio C, Zhou X, Neel BG, Pei D. 2011. Substrate specificity of protein tyrosine phosphatases 1B, RPTPα, SHP-1, and SHP-

2. *Biochemistry* **50**:2339–2356. doi:10.1021/bi1014453

Rice JJ, Daugherty PS. 2008. Directed evolution of a biterminal bacterial display scaffold enhances the display of diverse peptides. *Protein Eng Des Sel* **21**:435–442. doi:10.1093/protein/gzn020

Rube HT, Rastogi C, Feng S, Kribelbauer JF, Li A, Becerra B, Melo LAN, Do BV, Li X, Adam HH, Shah NH, Mann RS, Bussemaker HJ. 2022. Prediction of protein-ligand binding affinity from sequencing data with interpretable machine learning. *Nat Biotechnol*. doi:10.1038/s41587-022-01307-0

Rust HL, Thompson PR. 2011. Kinase consensus sequences: a breeding ground for crosstalk. *ACS Chem Biol* **6**:881–892. doi:10.1021/cb200171d

Schutkowski M, Reimer U, Panse S, Dong L, Lizcano JM, Alessi DR, Schneider-Mergener J. 2004. High-content peptide microarrays for deciphering kinase specificity and biology. *Angew Chem Int Ed* **43**:2671–2674. doi:10.1002/anie.200453900

Shah NH, Löbel M, Weiss A, Kuriyan J. 2018. Fine-tuning of substrate preferences of the Src-family kinase Lck revealed through a high-throughput specificity screen. *eLife* **7**:e35190. doi:10.7554/eLife.35190

Shah NH, Wang Q, Yan Q, Karandur D, Kadlecek TA, Fallahee IR, Russ WP, Ranganathan R, Weiss A, Kuriyan J. 2016. An electrostatic selection mechanism controls sequential kinase signaling downstream of the T cell receptor. *eLife* **5**:e20105. doi:10.7554/eLife.20105

Songyang Z, Blechner S, Hoagland N, Hoekstra MF, Piwnica-Worms H, Cantley LC. 1994a. Use of an oriented peptide library to determine the optimal substrates of protein kinases. *Curr Biol* **4**:973–982. doi:10.1016/s0960-9822(00)00221-9

Songyang Z, Carraway KL, Eck MJ, Harrison SC, Feldman RA, Mohammadi M, Schlessinger J, Hubbard SR, Smith DP, Eng C, Lorenzo MJ, Ponder BAJ, Mayer BJ, Cantley LC. 1995. Catalytic specificity of protein-tyrosine kinases is critical for selective signalling. *Nature* **373**:536–539. doi:10.1038/373536a0

Songyang Z, Shoelson SE, Chaudhuri M, Gish G, Pawson T, Haser WG, King F, Roberts T, Ratnofsky S, Lechleider RJ, Neel BG, Birge RB, Fajardo JE, Chou MM, Hanafusa H, Schaffhausen B, Cantley LC. 1993. SH2 domains recognize specific phosphopeptide sequences. *Cell* **72**:767–778.

Songyang Z, Shoelson SE, McGlade J, Olivier P, Pawson T, Bustelo XR, Barbacid M, Sabe H, Hanafusa H, Yi T. 1994b. Specific motifs recognized by the SH2 domains of Csk, 3BP2, fps/fes, GRB-2, HCP, SHC, Syk, and Vav. *Mol Cell Biol* **14**:2777–2785. doi:10.1128/mcb.14.4.2777-2785.1994

Stein A, Fowler DM, Hartmann-Petersen R, Lindorff-Larsen K. 2019. Biophysical and Mechanistic Models for Disease-Causing Protein Variants. *Trends Biochem Sci* **44**:575–588. doi:10.1016/j.tibs.2019.01.003

Sugiyama N, Imamura H, Ishihama Y. 2019. Large-scale Discovery of Substrates of the Human Kinome. *Sci Rep* **9**:10503. doi:10.1038/s41598-019-46385-4

Sweeney MC, Wavreille A-S, Park J, Butchar JP, Tridandapani S, Pei D. 2005. Decoding protein-protein interactions through combinatorial chemistry: sequence specificity of SHP-1, SHP-2, and SHIP SH2 domains. *Biochemistry* **44**:14932–14947. doi:10.1021/bi051408h

Tian H, Naganathan S, Kazmi MA, Schwartz TW, Sakmar TP, Huber T. 2014. Bioorthogonal fluorescent

labeling of functional G-protein-coupled receptors. *Chembiochem* **15**:1820–1829. doi:10.1002/cbic.201402193

Till JH, Annan RS, Carr SA, Miller WT. 1994. Use of synthetic peptide libraries and phosphopeptide-selective mass spectrometry to probe protein kinase substrate specificity. *J Biol Chem* **269**:7423–7428. doi:10.1016/S0021-9258(17)37302-7

Till JH, Chan PM, Miller WT. 1999. Engineering the substrate specificity of the Abl tyrosine kinase. *J Biol Chem* **274**:4995–5003. doi:10.1074/jbc.274.8.4995

Tinti M, Kiemer L, Costa S, Miller ML, Sacco F, Olsen JV, Carducci M, Paoluzi S, Langone F, Workman CT, Blom N, Machida K, Thompson CM, Schutkowski M, Brunak S, Mann M, Mayer BJ, Castagnoli L, Cesareni G. 2013. The SH2 domain interaction landscape. *Cell Rep* **3**:1293–1305. doi:10.1016/j.celrep.2013.03.001

Trinh TB, Xiao Q, Pei D. 2013. Profiling the substrate specificity of protein kinases by on-bead screening of peptide libraries. *Biochemistry* **52**:5645–5655. doi:10.1021/bi4008947

Uttamchandani M, Chan EWS, Chen GYJ, Yao SQ. 2003. Combinatorial peptide microarrays for the rapid determination of kinase specificity. *Bioorg Med Chem Lett* **13**:2997–3000. doi:10.1016/s0960-894x(03)00633-4

Wang X, Wei X, Yuan Y, Sun Q, Zhan J, Zhang J, Tang Y, Li F, Ding L, Ye Q, Zhang H. 2018. Src-mediated phosphorylation converts FHL1 from tumor suppressor to tumor promoter. *J Cell Biol* **217**:1335–1351. doi:10.1083/jcb.201708064

Wavreille A-S, Garaud M, Zhang Y, Pei D. 2007. Defining SH2 domain and PTP specificity by screening combinatorial peptide libraries. *Methods* **42**:207–219. doi:10.1016/j.ymeth.2007.02.010

Xie J, Supekova L, Schultz PG. 2007. A genetically encoded metabolically stable analogue of phosphotyrosine in Escherichia coli. *ACS Chem Biol* **2**:474–478. doi:10.1021/cb700083w

Yaffe MB, Leparc GG, Lai J, Obata T, Volinia S, Cantley LC. 2001. A motif-based profile scanning approach for genome-wide prediction of signaling pathways. *Nat Biotechnol* **19**:348–353. doi:10.1038/86737

Yeh RH, Lee TR, Lawrence DS. 2001. From consensus sequence peptide to high affinity ligand, a “library scan” strategy. *J Biol Chem* **276**:12235–12240. doi:10.1074/jbc.M011232200

Zheng Y, Gilgenast MJ, Hauc S, Chatterjee A. 2018. Capturing Post-Translational Modification-Triggered Protein-Protein Interactions Using Dual Noncanonical Amino Acid Mutagenesis. *ACS Chem Biol* **13**:1137–1141. doi:10.1021/acschembio.8b00021